Selective gas detection and quantification using a resistive sensor based on Pd-decorated soda-lime glass

Jin-Young Kim[a], Sang Sub Kim[a,*], Matteo Tonezzer[b,c,d, *]

[a] *Department of Materials Science and Engineering, Inha University, Incheon 22212, Republic of Korea*

[b] *IMEM-CNR, sede di Trento - FBK, Via alla Cascata 56/C, Povo (TN), Italy*

[c] *University of Trento, Via Calepina 14, Trento, Italy*

[d] *Department of Food Quality and Nutrition, Research and Innovation Centre, Fondazione Edmund Mach (FEM), San Michele all' Adige (TN), Italy*

[*] Corresponding authors.

E-mail addresses: sangsub@inha.ac.kr (S.S. Kim), matteo.tonezzer@cnr.it (M. Tonezzer).

ABSTRACT

A commercial soda-lime glass slide was decorated with palladium nanoparticles by UV light irradiation. The response, limit of detection, response and recovery times of the resistive gas sensor obtained were investigated at different temperatures (300-500°C) with four different gases (acetone, benzene, ethanol, and toluene). To overcome the main problem of this type of sensor (the lack of selectivity due to the one-dimensional output signal) a new approach was applied, which merges the sensor response values at different working temperatures. The responses obtained at five different temperatures (300-500°C), combined into 5-dimensional points, were then analyzed using a support vector machine. After a calibration with a training dataset, the detection system was able to accurately classify (recognize the gas) and quantify (estimate its concentration) all tested gases. The results showed that this sensing system achieved perfect classification (100%) and a good estimation of the concentration of tested gases (average error <19% in the range 1-30 ppm). These performance demonstrate that with our approach (different temperatures and machine learning) a single resistive sensor made of glass can achieve true selectivity and good quantification, while remaining much simpler, smaller and cheaper than an electronic nose.

Keywords: Gas sensor, Soda-lime glass, Pd, Selectivity, Machine learning

1. Introduction

The detection of volatile compounds and gases in different places (work, home, car interiors, hospitals, etc.) is increasingly important because of the pollution related to urbanization and industrialization. A capillary network of sensors is important in agriculture [1], food and beverage quality control [2], security against terrorism [3], and medical diagnosis [4].

Metal oxide semiconductors (MOS) are being used extensively as gas sensors because of their high sensitivity to a wide range of gases and compounds and relatively simple detection mechanism, providing an easily processable signal. MOS nanostructures are the last and best generation of such devices because their huge surface-to-volume ratio gives them a very high active interface with gas particles, thereby increasing their response [5]. In addition, the properties of the sensors can be tuned by changing the size and shape of MOS nanostructures because of their structure-dependent behavior [6,7]. Unfortunately, the stability of these nanostructures to temperature and humidity requires improvement. Different approaches, such as hybrid nanostructures [8,9] and surface decoration with catalytic noble metal nanoparticles, have been used to improve the sensitivity and selectivity of MOS gas sensors [10,11]. Metal nanoparticles work through two effects: chemical and electronic sensitization. In the first case, the metal has catalytic activity that depends on the gas being detected, as well as its dissociation and adsorption. In the second case, a Schottky barrier is formed at the interface between the two materials, and the modulation of its height greatly improves the sensor response.

Most substrates used for such devices are silicon or glass [12,13]. Recently, glass has also been investigated as a sensing material because it is inexpensive and can be worked easily with microelectronics techniques. This way, the glass can act as both the structural substrate and active sensing material. Porous glass was impregnated through two-step coloration reactions to obtain an optical sensor that can detect ppb-levels of NO_2 [14]. A thin film of fast

proton-conducting glass was used to fabricate solid-state potentiometric hydrogen and methanol sensors that can work at room temperature [15,16]. Peres et al. used glass material as a resistive sensor for the first time in 2018, demonstrating its ability to discriminate different VOC vapors [17]. The sensing mechanism of soda-lime glass was recently investigated. The results showed that the glass polarization is affected by the reaction of gaseous species on its surface [18]. Because the diffusion of ions inside the glass is a thermally activated effect, the sensing performance is expected to change with working temperature. A recent study focused on the functionalization of soda-lime glass with different noble metal nanoparticles to compare their sensing performance [19].

Unfortunately, the main problem with this type of sensor whose output signal is one-dimensional (for example current or voltage) is that the response is a pure number, and therefore inherently non-selective. For this reason, a resistive sensor works well only in limited conditions, when the gas to be measured is only one. To overcome this defect, numerous sensors based on different materials are often used together in an array, in order to increase the dimensionality and therefore the information that the sensing system gives out [20,21]. This is the approach used in *electronic noses*, which have attracted considerable interest [22-24]. Unfortunately, this traditional approach in electronic noses requires separate electrical connections for each sensor and different conditions for each material (metal oxides need high temperatures, polymers and small conjugated molecules need low temperatures, etc.) and this makes them complex, large, and expensive.

Therefore, a different approach was used in this study to achieve true selectivity while keeping the complexity and size of the device low: different temperatures were used instead of different materials [25,26]. In this novel approach, the responses obtained at different working temperatures were combined (similar to how the responses from different materials are combined in traditional electronic noses), and processed through machine learning algorithms [27,28].

Specifically, in this study a single slide of soda-lime glass was functionalized with Pd nanoparticles and used at the same time as a substrate and sensing material between interdigitated metal electrodes. The sensor responses at different temperatures (300–500°C) were combined in a more informative five-dimensional 5D output that was processed using a machine-learning algorithm (support vector machine, SVM). Each 5D point was the combination of five responses at the same concentration of the same gas, but collected at different working temperatures. A first dataset of 5D points was used to train the system (a kind of calibration), while a second dataset of 5D data was used to test the sensor performance.

The detection system obtained a perfect classification (accuracy and specificity = 100%) of the four tested gases (acetone, benzene, ethanol and toluene) and a good estimate of their concentrations (error <19% for concentrations above 1 ppm). These results demonstrate that by exploiting the response at different temperatures, real selectivity can be achieved using only a simple soda-lime glass based resistive sensor.

2. Experimental

2.1. Preparation of the Pd-functionalized soda-lime glass

Soda-lime glass microscope slides were purchased from Knittel-Gläser (Germany). The soda-lime glass surface was functionalized by dipping the slides into a solution of $PdCl_2$ dissolved in deionized water (Fig. 1b). The glass slides were then irradiated with 0.11 mW/cm^2 of UV light for 1 s (Fig. 1c). The short irradiation time (like the choice of Pd functionalization) was determined from an optimization step recently reported [19]. Finally, to remove residual solvents and improve the crystallization of the Pd nanoparticles functionalized on soda-lime glass slides, the samples were annealed at 500°C for 30 min (Fig. 1d). The sensing material was ready at the end of these steps (Fig. 1e).

2.2. Characterization

The morphology of the functionalized glasses was examined by field emission scanning electron microscopy (FE-SEM, JEOL 7600 F). The elemental composition of the Pd-glass slide was investigated by energy-dispersive X-ray spectroscopy (EDX) incorporated in the FE-SEM. The hysteresis I-V loops were measured using a Keithley 2400 sourcemeter.

2.3. Gas sensing test

The gas sensor was fabricated by depositing interdigitated electrodes (Pt over Ti, with a thickness of 200 and 50 nm, respectively) by DC sputtering on the glass surface through shadow masks (Fig. 1f,g). The two comb-like electrodes had seven fingers with a width of 400 microns and a gap of 400 microns between them (Fig. 1h,i). The two metal electrodes were connected to a Keithley 2400 Sourcemeter, and a constant DC bias of 1 V was applied. The current flowing through the sensing material was used to calculate the dynamic response of the sensor. The sensor was then inserted into a horizontal-quartz oven that could be heated to several hundred degrees Celsius. Pure synthetic dry air was flowed into the chamber for 30 min while the sensor was kept at a constant DC bias of 1 V to stabilize its signal. Each target gas (acetone, benzene, ethanol, and toluene) was then injected cyclically into the sensing chamber, while maintaining a total flow rate of 500 sccm. The sensor response was calculated as I_g/I_a, where I_g is the current in the presence of a target gas, and I_a is the current flowing through the sensor in dry air.

3. Results and discussion

3.1. Characterization of the Pd-functionalized glass

The morphology of the glass slide before and after the functionalization with Pd nanoparticles was examined by FE-SEM, as shown in Fig. 2. Several Pd nanoparticles covered the glass surface homogeneously (Fig. 2b), which is in contrast to the smooth surface

of the bare glass shown in Fig. 2a. The particles had diameters in the range of 100–200 nm. This coverage was chosen because a previous study found it to be the most effective for improving the sensing properties of soda-lime glass [19]. EDX was carried out to confirm the chemical composition of the nanoparticles. Figs. 2c and d present the EDX spectra of the bare and Pd-functionalized glass samples, respectively. The evident peaks corresponding to Si, O, Na, Ca, Mg, and Al indicate that the samples are typical soda-lime glass. A peak from Pd was observed only for the Pd-functionalized sample, as shown in Fig. 2d, showing that the nanoparticles formed on the bare glass slide were Pd. Table S1 lists the chemical composition estimated from the integration area of a peak in the EDX spectra. The observed morphology and chemical composition confirmed that the functionalization process of the surface was successful.

3.2. Sensing mechanism of the Pd-functionalized glass

The electrical properties of the Pd-functionalized soda-lime glass sensor were investigated to understand the sensing mechanism. The results show that the sensor had significant electrical conductivities at high temperatures, as shown in Fig. 3. The hysteresis feature of the soda-lime glass sample appeared only at 300^{o}C, as shown in Fig. 3a. In addition, the maximum current during the I-V loops depends strongly on the sweeping speed, while showing a similar shape for various voltages at the same sweeping speed, as shown in Fig. 3b. This behavior indicates the accumulation of electrostatic surface charges by local electrochemical effects between the electrodes under bias [29,30].

Exponential capacitive decay was observed upon DC biasing (Fig. 3c), indicating that polarization developed in the Pd-functionalized soda-lime glass [31-33]. The three continuous runs took 30 minutes to reach a steady current of approximately 0.045 μA at 300°C and 1 V DC bias. At this stage, the maximum charge was stored between the electrodes by glass polarization [34,35]. The electrical charge eventually dissipates during a final continuous run,

i.e., 0 V-4th run in Fig. 3c. A significant negative current, ranging from -0.37 to -0.03 μA, flowed through the sourcemeter without an external bias for more than 500 s after the three continuous runs, eventually leading to an equilibrium zero current. The temperature-dependent hysteresis I-V loops (Fig. 3d) revealed the Arrhenius behavior [36] of the conductivity in the Pd-functionalized soda-lime glass sample. In our earlier report [18], the I-V characteristics of bare soda-lime glass were presented. For example, the I–V loop obtained at 1 V and sweeping rate of 120 s/sweep at 300^{o}C revealed a current of ±0.21 μA, corresponding to a resistance value of 4.76 MΩ. This confirms that the soda-lime glass without Pd decoration is quite insulating. The I-V loops obtained from the Pd-decorated soda-lime glass at the same condition revealed a current of ±0.12 μA, corresponding to a resistance value of 8.33 MΩ. This indicates that the Pd decoration makes a greater resistance value in comparison to the bare soda-lime glass.

A previous study described the gas sensing mechanism for the Pd-functionalized glass [19]. Under high working temperatures, alkali ions with a positive charge in the soda-lime glass can gain good mobility and rearrange themselves under an applied external electric field. This results in a concentration gradient of the cations, leading to the macroscopic glass polarization, as shown schematically in Fig. 4a. Under this circumstance, the output current (I) at a fixed applied voltage can be explained as $I=I_v-I_c$, where I_v and I_c are voltage- and charge-dependent current terms, respectively. Although I_v is dependent only on the applied voltage, I_c is strongly dependent on the number of mobile cations. When a bias voltage is applied, mobile alkaline positive ions, such as Na^+, are highly populated near the cathode. Electrical neutral compounds (ENCs) were formed when a target gas was introduced to the glass sensor, reducing the polarization of the glass sensor. Accordingly, I_c decreases, which can explain the increase in total current when a target gas is introduced.

As illustrated in Fig. 4b, Pd nanoparticles can play a catalytic role in facilitating the

decomposition of target gas molecules and providing a spillover effect, leading to more surface reactions. Hence, more ENCs were generated, and I_c is reduced further. This is why Pd functionalization gives an increased output current, resulting in an enhanced gas response. In our earlier work [19], the specific effects of metal decoration such as Pd, Pt and Au on soda-lime glass were investigated. The gas sensing results revealed that Pd functionalization leads to a relatively high selectivity to benzene. This selective sensing property was explained by the adsorption energy of benzene onto Pd. The experimental adsorption energy of benzene onto Pd was 1.35 eV, which is a good value for easy adsorption and desorption in comparison with the values of other metals.

As shown in Fig. S2, sensing properties toward hydrogen and ammonia gases of the Pd-decorated soda-lime glass sensor were also tested. Regardless of the well-known effect of Pd on hydrogen sensing capability, the sensor in this work showed a superior benzene-sensing capability in comparison with all other tested gases such as ethanol, acetone, toluene, hydrogen, and ammonia at the optimized operating temperature of 350^{o}C.

3.3. Dynamic current and traditional selectivity

The Pd-functionalized glass sensor was exposed to different concentrations of acetone, benzene, ethanol, and toluene gas, as listed in Table S2. The background color of the columns will be important in the next section, when it will be used to explain the machine learning post-processing.

As a first step, the dynamic current passing through the sensor was measured during a few gas cycles at different concentrations. All the plots showed similar behavior (Fig. 5), with the dynamic current increasing steeply when the gas was injected and then decreasing when the gas was expelled. The current increased significantly with increasing gas concentration. In all cases, the current returned to its previous value, proving the reversibility of the sensor response. During each peak (a period in which the gas concentration was constant), the sensor

current tended to drop more or less noticeably. This did not affect the sensor operation because the decrease was slow compared to the sensor response and recovery times.

The sensor responses for each gas were calculated from Fig. 5, as described in Section 2.3. Fig. 6 presents the results for 100 ppm for each gas. Typically, these measurements are used to determine the optimal working temperature for a sensor to maximize its response. In the present case, these data are much more important. The responses towards all gases reached their maximum at the same temperature: 350°C. The sensor stability was tested by measuring the dynamic sensing curve for repeated cycles of 10 ppm benzene gas at 350°C, and the result is shown in Fig. S1. It shows that the sensor responses fall in a reasonable error range for five measurements, evidently demonstrating the good sensor stability. More important than the temperature at which the maximum response is obtained, is the internal structure between the bars at 350°C, showing that the selectivity also reached its maximum at this temperature. Note that the selectivity is traditionally defined as the lowest value among the partial selectivities, which were calculated on each couple of gases [37]. For example, at all temperatures the sensor was selective to benzene, with toluene being the first interferer (except at 350°C). At 350°C, the responses of both ethanol and benzene increased considerably; the sensor was still selective to benzene, but the first interferer, in this case, was ethanol. The selectivity of benzene towards the other interfering gases was as follows: 4.3 (acetone), 2.25 (ethanol), and 3.7 (toluene). Therefore, the overall selectivity of the sensor at 350°C was 2.25. The selectivity was calculated at different temperatures to confirm the best selectivity of the sensor, as listed in Table 1.

The selectivity at 350°C was the best for the glass sensor, which showed more than double the response to benzene than to ethanol. A situation like the one in Fig. 2 at 350°C was much better than that at 300°C because the sensor responds much more intensely to a single gas than to the other gases.

Nevertheless, if one of the tested gases is injected on the sensor without knowing which

one, there is no information as to which gas it is. Any response could be generated by a low concentration of benzene, a higher concentration of ethanol, or an even higher concentration of acetone or toluene. Therefore, a novel approach was applied, which uses the response values at different working temperatures as multidimensional data to be processed by machine learning algorithms to achieve real selectivity. This idea combines the different responses (obtained at different working temperatures) in more informative 5D points.

Each very informative 5D point contains the five response values and all the correlations among them. In other words, each 5D point summarizes one *thermal fingerprint* (response as a function of the working temperature), as shown in Fig. 7, and previously explained elsewhere [38,39].

Each plot in Fig. 7 is relative to one gas and can be used to recognize it with future measurements because its shape is characteristic of that gas. In a first step, a series of these fingerprints (in form of 5D points) was given to the sensing system to teach it how to recognize each gas (like a more complex calibration step). During this step, a set of 5D points was provided with two labels: the name of the gas and its concentration. The sensing system can learn the shape of each gas-specific fingerprint, and, by comparing the fingerprint of a new unknown measurement, recognize the gas in a new test. The second label (the gas concentration) is important because the fingerprint of each gas maintains the same shape, but changes with the gas concentration, as shown in Fig. 8.

Fig. 8 shows the thermal fingerprints obtained for different concentrations of ethanol gas. The shape of the fingerprint remains the same, but the intensity increases with increasing gas concentration. Owing to these two labels, the system can learn how to recognize each gas and subsequently estimate its concentration. Note that the system can be trained to recognize new gases and distinguish them. The system only needs a first training dataset for each gas, as for a simpler calibration step.

3.4. Principal component analysis (PCA)

Because the data used by the sensing system are 5-dimensional, it is impossible to visualize them on a screen or paper. To give the reader an idea of how the sensor works, a dimensions reduction was applied through principal components analysis (PCA). This unsupervised method is a statistical procedure, in which the data are fed to the system with no label. The procedure is used frequently to reduce the number of dimensions and allow the data to be visualized. This type of projection chooses the principal components as the orthogonal directions, maximizing the variance of each subsequent component.

Fig. 8 shows the first three principal components, helping to visualize the relationships among the points better. Each point in Fig. 9 is the reduction from a 5D point to a 3D point, which contains all the measurements of the same gas at the same concentration but at different working temperatures. Each segmented line in Fig. 7 or 8 is combined in a multidimensional point that is then minimized in a colored point in Fig. 9. Only the training points come with a label that identifies them as relating to a certain gas, which translates into a color in the PCA plot. A small dense cloud of cyan points, relative to air without any target gas, can be seen in the center of Fig. 9. The points cluster quite densely because there is no difference among them. Therefore, the different position rises only from the error on the raw signal from the sensor. Around this cyan cloud, the points relative to the target gases (acetone in red, ethanol in green, benzene in blue, and toluene in purple) lay on curved lines, quite far from each other. Owing to the PCA projection, they are well separated and easy to distinguish.

The fact that the points of each gas are not grouped in a small cloud (as is often reported) is not a weak point of this method. Points lying on lines instead of in small clouds make it more difficult to classify a system. However, this makes it possible to perform further analysis and obtain an estimate of the gas concentrations, as shown in section 3.6.

3.5. Classification of gases

As shown in the previous section, points relating to different gases occupy different regions of space. The points relating to the different gases are recognizable in Fig. 9, facilitating the classification of new unknown points based on their position with respect them. For example, a new gray dot from a new sensor measurement can be classified by looking at Fig. 9 and seeing near which line of dots it is placed. If it is close to the purple spots, the gas in question will likely be toluene. This assessment can be made using the human eye; however, the sensing system can work in five dimensions.

The core of the sensing discrimination and selectivity is a support vector machine, which is a supervised learning algorithm that produces a model consisting of 4D hyperplanes in 5D, which indicate the boundaries between 5D areas corresponding to different gases. This model is produced using a first dataset of training points (the ones shown in Fig. 9) to recognize the regions of 5D space "belonging" to each target gas.

Any new data (the points with a white background in Table S2) are compared by the system with the trained model to classify it. Table 2 lists the confusion matrix of the sensor classification; each row is related to the actual gas in the sensing chamber, while each column is giving the gas that the sensing system has identified. This means that the numbers on the diagonal of the matrix are correctly identified measurements, while those outside are misclassified. As listed in Table 2, the Pd-decorated soda-lime glass sensors performed perfect classification, with an accuracy and a specificity of 100%. This proves that the SVM, working in 5D space, discriminates even better than the human eye with only a three-dimensional plot in Fig. 9.

As shown in Fig. S3, the sensor was also tested with a 50-50% mixture of benzene and toluene, in order to verify if the system is able to distinguish and quantify even gas mixtures. As can be seen, the points relating to the two gases and the mixture are well separated, and follow distinct lines. It should be emphasized that the concentration, in all three cases, increases from bottom to top in the figure (from 1 to 100 ppm). The first step carried out by

the sensor is to distinguish the two gases and the mixture. A support vector machine acts as a classifier, and recognizes (using a first series of "calibration" points) the areas of the 5D space where the points relating to benzene, toluene and the mixture are located. In this way, each new measurement made with the sensor is automatically labeled by the system, which recognizes what is present in the measurement chamber, whether it is gas or mixture.

3.6. Estimation of gas concentration

The previous section showed that the sensing system can perfectly classify the test gases, even if the new measurements are taken at different concentrations. In other words, the sensor can distinguish the 5D space areas related to each gas, even if the points of each gas in Fig. 9 are very far from each other. This arrangement of points makes the classification more difficult, but it can achieve a further objective, which is illustrated and explained. Small and dense clouds of points from PCA plots (unlike in Fig. 9) can be managed easily using untrained methods, relying on the distance between points. On the other hand, this arrangement makes it impossible to differentiate the points belonging to the same gas at different concentrations.

Because the points in Fig. 9 are distant and positioned on lines, a support vector regressor can be used to estimate the gas concentration of each point [40,41]. This step must be done after the previous one because the system needs to know how the gas has been classified. As in the previous section, the classification occurs using four different combined dual classifiers; here, four regressors are used, one for each gas. Each SV regressor is trained with the data classified for that gas, using their concentration label. Each new point is sent to the regressor chosen by its classification. An incorrect classification would often lead to an incorrect estimate of the concentration.

The sensing system can understand which gas is present and its concentration, even though that gas has not been tested at that specific concentration. Fig. 10 presents the support

vector regression results, where each gas is plotted in a different color. As already mentioned, if a point is classified incorrectly in the previous step, it would be plotted with a different (incorrect) color.

The points in Fig. 10 indicate the regression results: the concentration estimate versus the real concentration of the gas. The true concentrations (on the abscissas) correspond to those of the test points (those with a white background in Table S2). The quality of the regressor estimates is easy to evaluate in Fig. 10 because the diagonal indicates the perfect estimate, which corresponds to the true concentration. As shown in Fig. 10, the points relative to all four gases are laying close to the diagonal, meaning that the estimated concentrations are good. The mean percentage error for each gas was calculated to quantify how good the concentration estimate is, as listed in Table 3.

The test points were chosen to be alternating with those used to teach the model, as listed in Table S2. In this way, the test points are as far as possible from the reference points, and the error is the maximum achievable. This means that measurements of random concentrations (a more realistic case) would be characterized by a smaller error. Benzene and ethanol showed larger errors than acetone and toluene. The sensor could not detect acetone at sub-ppm concentrations; thus, the point at 0.2 ppm is missing for acetone. The error was strongly affected by the points on the left (Fig. 9). Indeed, the error has a common trend for most gases; it is higher at low concentrations, lower in the middle, and larger (but less) at higher concentrations.

Two effects can explain this: i) the calibration border and ii) the proximity to the limit of detection [42]. The support vector machine model works like a calibration; it works worse away from trained concentrations. Hence, the model is weaker approaching the border of the trained interval, and the error is larger. This occurs at both extremities of the tested concentrations range. Furthermore, the limit of detection of the sensor is being approached on the left of Fig. 10. Therefore, the raw response of the resistive sensor gradually loses its

meaning. This second effect adds to the first, further enlarging the error of the estimate.

The analysis can be limited to this concentration interval, given that most of the hazard thresholds are in the ppm range. If the average percentage error leaving out the points below 1 ppm can be calculated, the sensing system is much more precise, as shown in Table 4. Considering only the concentrations above 1ppm, the average percentage errors are 13.2%, 29.4%, 18.2%, and 14.7% for acetone, benzene, ethanol, and toluene, respectively. In addition, as shown in Fig. S4, The error on the measurement of the mixture concentration (14.4%) is comparable to that made on the single gases (benzene 13.3%, toluene 8.5%). Such errors are acceptable, especially considering that the dangerousness of the various gases varies with the order of magnitude of the concentration and not with the individual ppm.

These results indicate that this is not a theoretical technique, because it has proven to be able to discriminate individual gases perfectly (100% correct classification) in the case of real measurements, even in double blind conditions. It is also worth pointing out that with this technique the sensor system makes decisions autonomously, without the need for the presence of a human operator.

4. Conclusions

A resistive gas sensor based on Pd-decorated soda-lime glass with metal interdigitated electrodes was fabricated and used to detect four different reducing gases (acetone, benzene, ethanol, and toluene). The response values obtained at five different working temperatures (300-500°C in steps of 50°C) were combined in highly informative 5-dimensional points, which were then processed using machine learning algorithms. Using a support vector machine as a classifier and then as a regressor, one single sensor was able to discriminate all four gases perfectly (100%) and estimate their concentrations with an average error <19%. With this novel approach that uses one single sensor at different temperatures instead of several sensors of different materials, it was possible to achieve true selectivity and good

quantification with a much smaller, simpler and cheaper detection system than a traditional electronic nose. This could allow the widespread diffusion of tiny selective sensors integrated into portable devices and networked, enabling to monitor the environment much more effectively.

Acknowledgments

This study was supported by Inha University and the Institute of Materials for Electronics and Magnetism (IMEM-CNR).

Appendix A. Supplementary data

Supplementary data associated with this article can be found in the online version at http://dx.doi.org/

References

[1] A.A. Makky, A. Alaswad, D. Gibson, A.G. Olabi, Renewable energy scenario and environmental aspects of soil emission measurements, Renewable Sustainable Energy Rev. 68 (2017) 1157–1173.

[2] D. Barreca, A. Gasparotto, F. Gri, E. Comini, C. Maccato, Plasma-assisted growth of β–MnO_2 nanosystems as gas sensors for safety and food industry applications, Adv. Mater. Interfaces 5 (2018) 1800792.

[3] Y. Ge, Z. Wei, Y. Li, J. Qu, B. Zu, X. Dou, Highly sensitive and rapid chemiresistive sensor towards trace nitro-explosive vapors based on oxygen vacancy-rich and defective crystallized In-doped ZnO, Sens. Actuators B Chem. 244 (2017) 983–991.

[4] M. Righettoni, A. Amann, S.E. Pratsinis, Breath analysis by nanostructured metal oxides as chemo-resistive gas sensors, Mater. Today 18 (2015) 163-171.

[5] A. Mirzaei, S.S. Kim, H.W. Kim, Resistance-based H_2S gas sensors using metal oxide nanostructures: A review of recent advances, J. Hazard. Mater. 357 (2018) 314–331.

[6] B.-Y. Wang, D.-S. Lim, Y.-J. Oh, CO gas detection of Al-doped ZnO nanostructures with various shapes, Jpn. J. Appl. Phys. 52 (2013) 101103.

[7] M. Tonezzer, T.T.L. Dang, N. Bazzanella, V.H. Nguyen, S. Iannotta, Comparative gas-sensing performance of 1D and 2D ZnO nanostructures, Sens. Actuators B Chem. 220 (2015) 1152–1160.

[8] I.S. Jeon, G. Bae, M. Jang, W. Song, S. Myung, S.S. Lee, H.-K. Jung, J. Hwang, K.-S. An, A synergistic combination of zinc oxide nanowires array with dual-functional zeolitic imidazolate framework-8 for hybrid nanomaterials-based gas sensors, Compos. B. Eng. 180 (2020) 107552.

[9] J. Hu, M. Chen, Q. Rong, Y. Zhang, H. Wang, D. Zhang, X. Zhao, S. Zhou, B. Zi, J. Zhao, J. Zhang, Z. Zhu, Q. Liu, Formaldehyde sensing performance of reduced graphene oxide-wrapped hollow SnO_2 nanospheres composites, Sens. Actuators B Chem. 307 (2020) 127584.

[10] J.-H. Lee, A. Mirzaei, J.-Y. Kim, J.-H. Kim, H.W. Kim, S.S. Kim, Optimization of the surface coverage of metal nanoparticles on nanowires gas sensors to achieve the optimal sensing performance, Sens. Actuators B Chem. 302 (2020) 127196.

[11] A. Katoch, S.-W. Choi, G.-J. Sun, S.S. Kim, Low temperature sensing properties of Pt nanoparticle-functionalized networked ZnO nanowires, J. Nanosci. Nanotechnol. 15 (2015) 330-333.

[12] V.V. Petrov, A.P. Starnikova, Y.N. Varzarev, K.A. Abdullin, D.P. Makarenko, Gas sensitive properties of ZnO nanorods formed on silicon and glass substrates, IOP Conf. Ser., Mater. Sci. Eng. 703 (2019) 012038.

[13] R. Prajesh, V. Goyal, V. Saini, J. Bhargava, A. Sharma, A. Agarwal, Development and reliability analysis of micro gas sensor platform on glass substrate, Microsyst. Technol.

25 (2019) 3589-3597.

[14] T. Tanaka, A. Guilleux, T. Ohyama, Y.Y. Maruo, T. Hayashi, A ppb-level NO_2 gas sensor using coloration reactions in porous glass, Sens. Actuators B Chem. 56 (1999) 247–253.

[15] M. Nogami, M. Matsumura, Y. Daiko, Hydrogen sensor prepared using fast proton-conducting glass films, Sens. Actuators B Chem. 120 (2006) 266–269.

[16] M. Nogami, T. Maeda, T. Uma, A methanol gas sensor based on inorganic glass thin films, Sens. Actuators B Chem. 137 (2009) 603–607.

[17] H.E.M. Peres, E. Galeazzo, M.O.S. Dantas, W. Beccaro, G.P. Filbrich, F.J. Ramirez-Fernandez, Evaluation of the electrical resistance response of insulating glass surface to sense and classify humidity and VOCs vapors, IEEE Sens. J. 18 (2018) 3940-3945.

[18] K.V. Sopiha, J.-H. Kim, S.S. Kim, P. Wu, Gas sensing properties of standard soda-lime glass, Sens. Actuators B Chem. 266 (2018) 344–353.

[19] J.-Y. Kim, A. Mirzaei, J.-H. Kim, J.-H. Lee, H.W. Kim, S.S. Kim, Incorporation of metal nanoparticles in soda-lime glass sensors for enhancing selective sensing, Sens. Actuators B Chem. 296 (2019) 126673.

[20] C.S. Prajapati, S. Benedict, N. Bhat, An ultralow power nanosensor array for selective detection of air pollutants, Nanotechnol. 31 (2019) 025301.

[21] S. Khaldi, Z. Dibi, Neural network technique for electronic nose based on high sensitivity sensors array, Sens. Imaging 20 (2019) 15.

[22] E.N. Carmona, V. Sberveglieri, A. Ponzoni, V. Galstyan, D. Zappa, A. Pulvirenti, E. Comini, Detection of food and skin pathogen microbiota by means of an electronic nose based on metal oxide chemiresistors, Sens. Actuators B Chem. 238 (2017) 1224–1230.

[23] H.G. Moon, Y. Jung, S.D. Han, Y.-S. Shim, B. Shin, T. Lee, J.-S. Kim, S. Lee, S.C. Jun, H.-H. Park, C. Kim, C.-Y. Kang, Chemiresistive electronic nose toward detection of biomarkers in exhaled breath, ACS Appl. Mater. Interfaces 8 (2016) 20969-20976.

[24] S. Jiang, J. Wang, Y. Wang, S. Cheng, A novel framework for analyzing MOS E-nose data based on voting theory: Application to evaluate the internal quality of Chinese pecans, Sens. Actuators B Chem. 242 (2017) 511–521.

[25] M. Tonezzer, D.T.T. Le, T.Q. Huy, S. Iannotta, Dual-selective hydrogen and ethanol sensor for steam reforming systems, Sens. Actuators B Chem. 236 (2016) 1011–1019.

[26] M. Tonezzer, Selective gas sensor based on one single SnO_2 nanowire, Sens. Actuators B Chem. 288 (2019) 53-59.

[27] T.M. Ngoc, N.V. Duy, C.M. Hung, N.D. Hoa, H. Nguyen, M. Tonezzer, N.V. Hieu, Self-heated Ag-decorated SnO_2 nanowires with low power consumption used as a predictive virtual multisensor for H_2S-selective sensing, Anal. Chim. Acta 1069 (2019) 108-116.

[28] M. Tonezzer, L.T.T. Dang, H.Q. Tran, S. Iannotta, Multiselective visual gas sensor using nickel oxide nanowires as chemiresistor, Sens. Actuators B Chem. 255 (2018) 2785–2793.

[29] R. Proksch, Electrochemical strain microscopy of silica glasses, J. Appl. Phys. 116 (2014) 066804.

[30] R.K. Vasudevan, N. Balke, P. Maksymovych, S. Jesse, S.V. Kalinin, Ferroelectric or non-ferroelectric: Why so many materials exhibit “ferroelectricity” on the nanoscale, Appl. Phys. Rev. 4 (2017) 021302.

[31] A. Wikby, G. Johansson, The resistance and intrinsic time constant of glass electrodes, J. Electroanal. Chem. Interf. Electrochem. 23 (1969) 23-40.

[32] K. Tamamoto, H. Namikawa, Conduction current relaxation of inhomogeneous conductor I, Jpn. J. Appl. Phys. 27 (1988) 1845.

[33] R.J. Charles, Polarization and diffusion in a silicate glass, J. Appl. Phys. 32 (1961) 1115-1126.

[34] A. Doi, Alkali motion in alkali silicate glass, J. Appl. Phys. 50 (1979) 1291-1297.

[35] C. McLaren, B. Roling, R. Raj, H. Jain, Mechanism of electric field-induced softening (EFIS) of alkali silicate glasses, J. Non Cryst. Solids 471 (2017) 384-395.

[36] H. Mehrer, Diffusion in Solids: Fundamentals, Methods, Materials, Diffusion-controlled Processes, Springer Science & Business Media, New York, 2007.

[37] W. Göpel, K.D. Schierbaum, Sensors: A comprehensive survey (City Publishers), vol. 2, VCH Publishers, New York, 1991.

[38] M. Tonezzer, T.T.L. Dang, Q.H. Tran, V.H. Nguyen, S. Iannotta, Selective hydrogen sensor for liquefied petroleum gas steam reforming fuel cell systems, Int. J. Hydrog. Energy 42 (2017) 740-748.

[39] M. Tonezzer, J.-H. Kim, J.-H. Lee, S. Iannotta, S.S. Kim, Predictive gas sensor based on thermal fingerprints from Pt-SnO_2 nanowires, Sens. Actuators B Chem. 281 (2019) 670-678.

[40] S. Xu, X. An, X. Qiao, L. Zhu, L. Li, Multi-output least-squares support vector regression machines, Pattern Recognit. Lett. 34 (2013) 1078–1084.

[41] M. Tonezzer, D.T.T. Le, S. Iannotta, N.V. Hieu, Selective discrimination of hazardous gases using one single metal oxide resistive sensor, Sens. Actuators B Chem. 277 (2018) 121-128.

[42] M. Tonezzer, S.C. Izidoro, J.P.A. Moraes, L.T.T. Dang, Improved gas selectivity based on carbon modified SnO_2 nanowires, Front. Mater. 6:277. https://doi.org/10.3389/fmats.2019.00277.

Table and Figure Captions

Table 1. Selectivity measured at different working temperatures.

Table 2. Confusion matrix for the testing points (in each row, there is the true gas, while in each column, there is the gas identified by the sensing system).

Table 3. Average percentage error calculated for each gas.

Table 4. Average percentage error calculated for each gas, limited to concentrations greater than 1 ppm.

Fig. 1. Process steps to obtain the sensing material (a-e) and steps to fabricate the sensing device (f-i). (a) Commercial soda-lime slide, b) immersion in solution, c) irradiation with UV light, d) annealing at 500°C, e) Pd-functionalized soda-lime glass. f) deposition of an adhesion layer of Ti, g) deposition of the Pt electrode, h) final sensor, i) cross-section of the sensor to show the different materials.

Fig. 2. FE-SEM images and EDX spectra of the bare glass (a and c) and Pd-functionalized glass (b and d) surfaces, respectively.

Fig. 3. Electrical characteristics of the Pd-functionalized soda-lime glass: (a) Normalized hysteresis I-V loops using at different temperatures in a continuous sequence from 100 to 300^{o}C with 120 s/sweep sweeping speed. (b) Hysteresis I-V loops for various sweeping speeds measured in a continuous sequence from 12 to 120 s/sweep at 300^{o}C. The inset presents the hysteresis I-V loops obtained at various sweeping voltages in a continuous sequence from 0.5 to 5 V using sweeping speed for 120 s/sweep at 300^{o}C. (c) Capacitive decays of current obtained under 1 V DC bias for three continuous runs, followed by the fourth unbiased run at 300^{o}C. (d) Temperature dependence of the electrical conductance. The data points represent the corresponding conductance values calculated with the current I values during the I-V sweeping at various temperatures.

Fig. 4. Schematic illustration of the sensing mechanism of Pd-functionalized soda-lime glass: (a) Macroscopic glass polarization under external electric field and cation change by the target gas in a bare glass. (b) Catalytic effect by Pd functionalization after the introduction of the target gas.

Fig. 5. Plots of the dynamic current measured at different temperatures for different gases at

different concentrations.

Fig. 6. Sensor response to 100 ppm of each gas, measured at different temperatures.

Fig. 7. Thermal fingerprints (sensor response as a function of working temperature) relative to each gas, measured at a concentration of 100 ppm.

Fig. 8. Thermal fingerprints (sensor response as a function of the working temperature) relative to different concentrations of ethanol gas.

Fig. 9. Three-dimensional plot of the first three principal components, showing the data relative to the different gases in different colors.

Fig. 10. Concentration estimate by the sensing system (Y-axis) versus real concentration (X-axis). Perfect estimates lay on the diagonal.

Table 1. Selectivity measured at different working temperatures.

Temperature	300°C	350°C	400°C	450°C	500°C
Target gas	benzene	benzene	benzene	benzene	benzene
First interferer	toluene	ethanol	toluene	toluene	toluene
Selectivity	1.17	2.25	1.19	1.06	1.005

Table 2. Confusion matrix for the testing points (in each row, there is the true gas, while in each column, there is the gas identified by the sensing system).

	Acetone	Air	Benzene	Ethanol	Toluene
Acetone	2				
Air		5			
Benzene			3		
Ethanol				3	
Toluene					3

Table 3. Average percentage error calculated for each gas.

Gas	Acetone	Benzene	Ethanol	Toluene
% Error	17.9	63.9	70.6	15.4

Table 4. Average percentage error calculated for each gas, limited to concentrations greater than 1 ppm.

Gas	Acetone	Benzene	Ethanol	Toluene
% Error	13.2	29.4	18.2	14.7

Figure 1

Click here to access/download;Figure(s);Fig. 1.tif

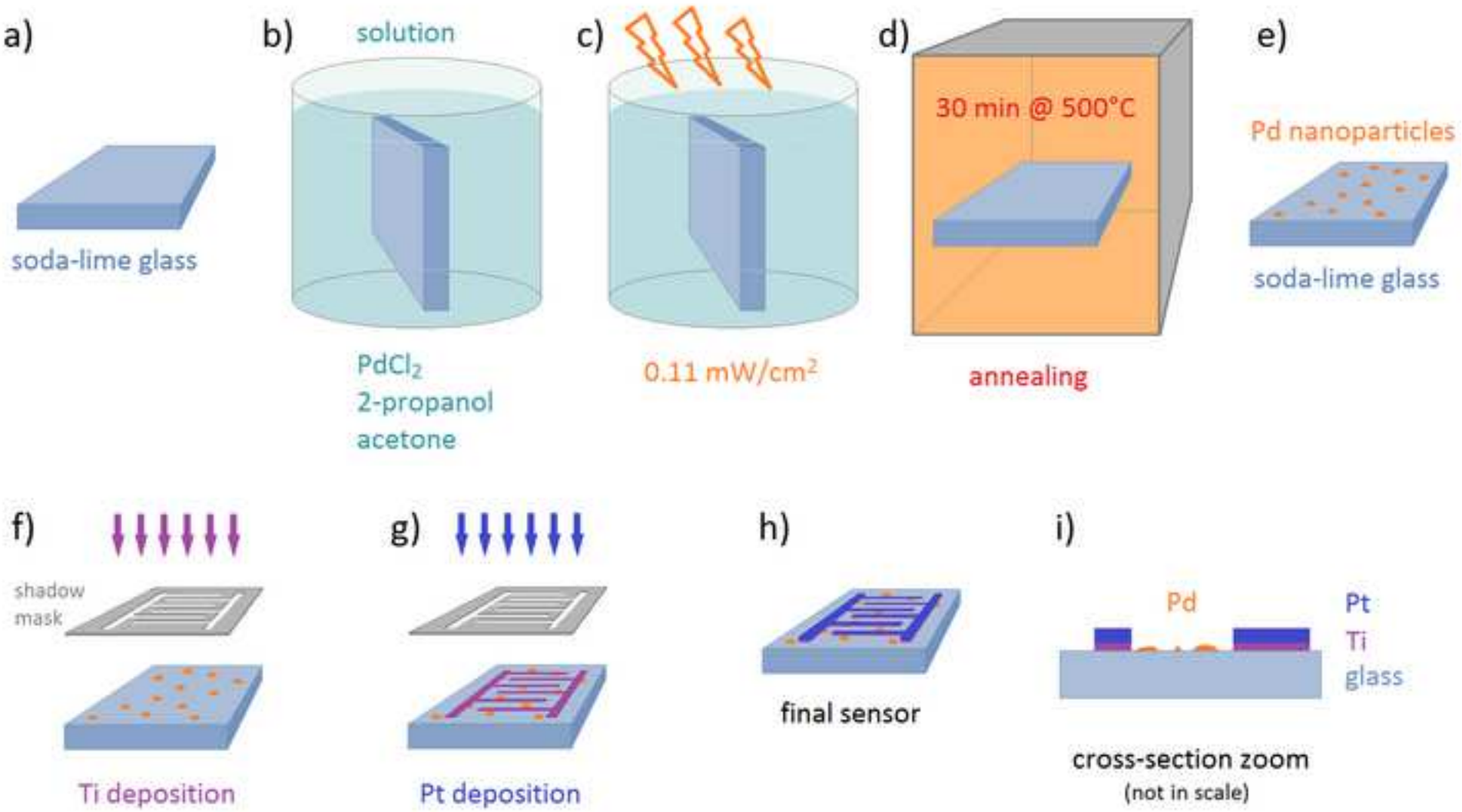

Figure 2

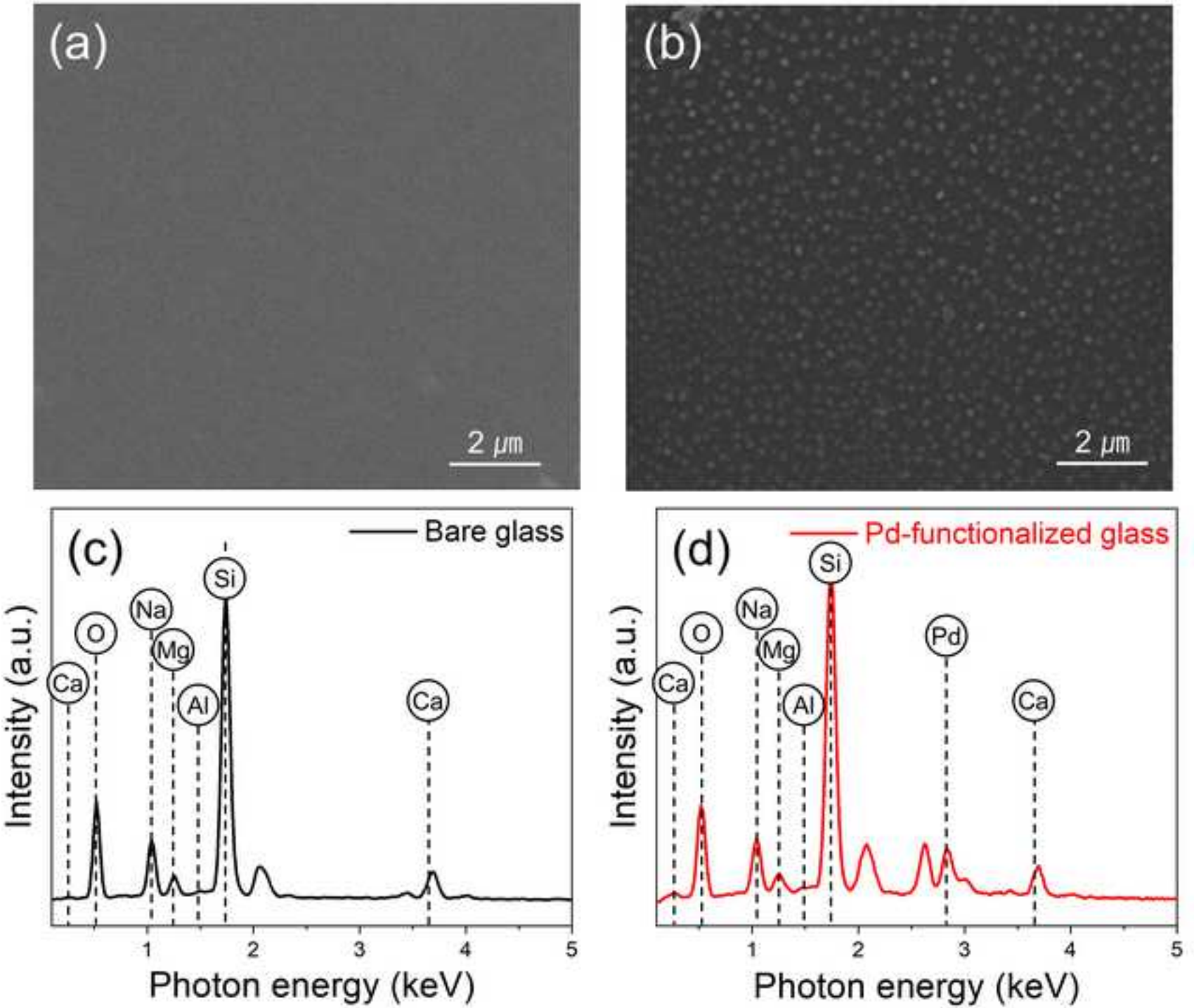

Figure 3

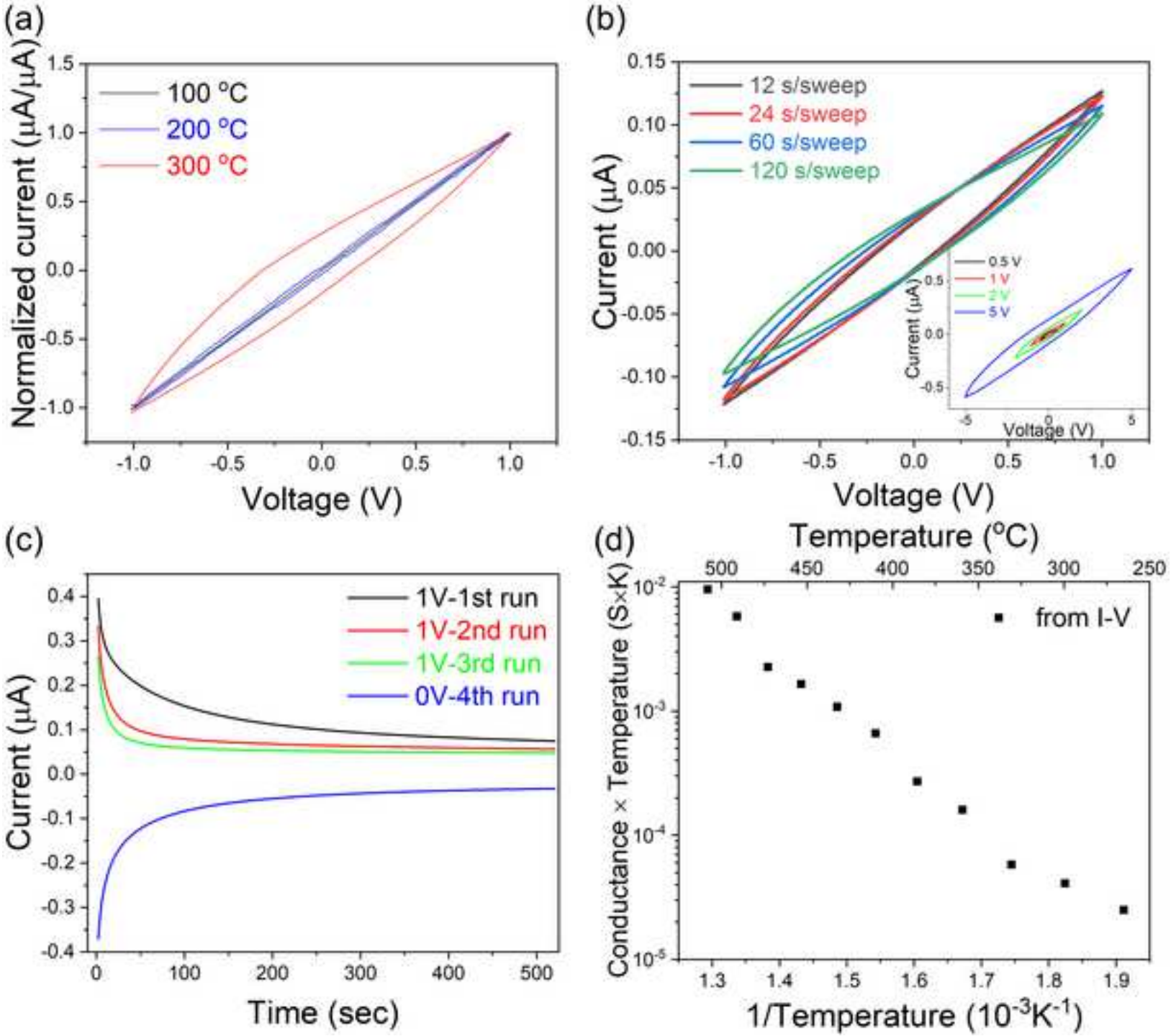

Figure 4

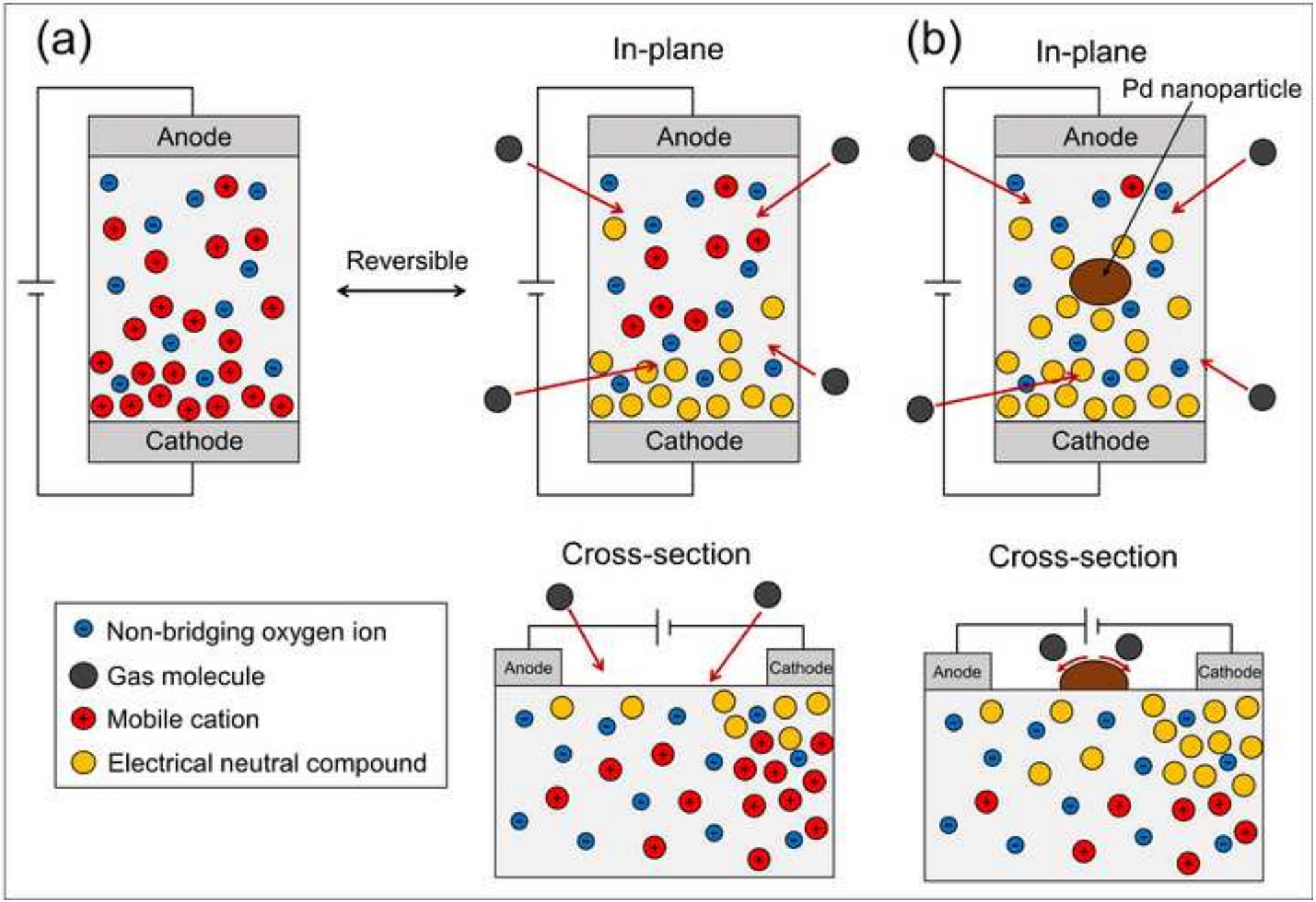

Figure 5

Click here to access/download;Figure(s);Fig. 5.tif

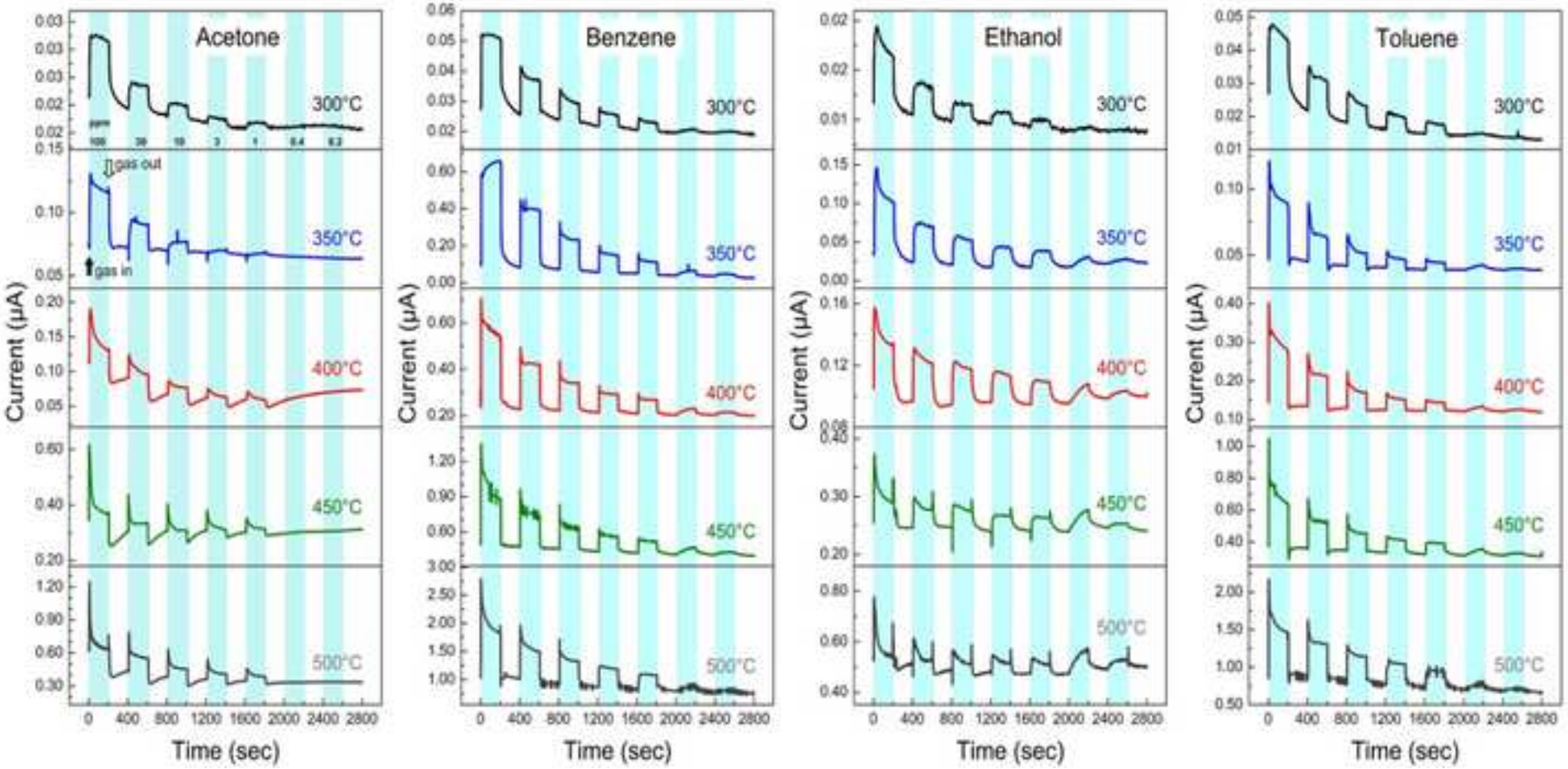

Figure 6

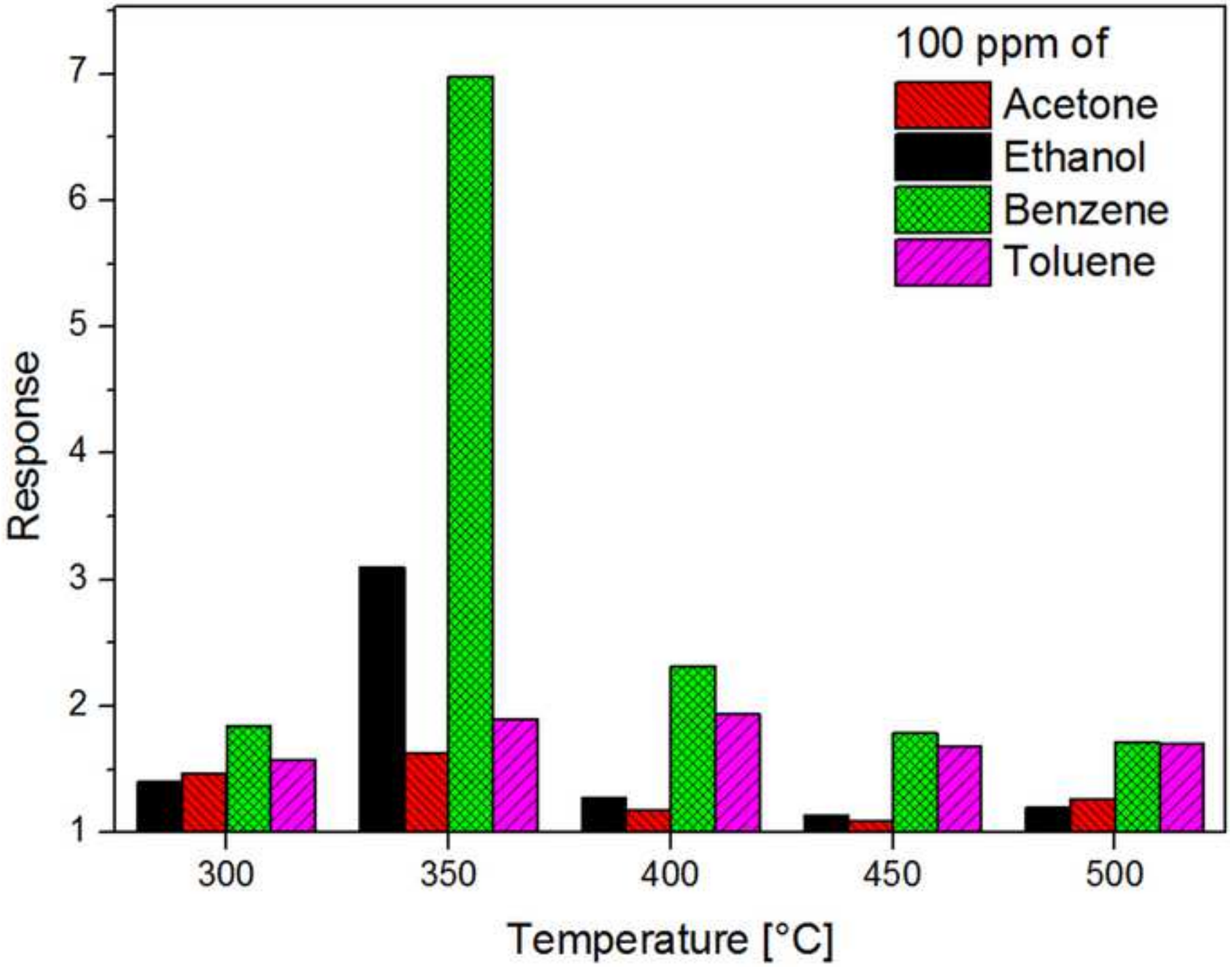

Figure 7

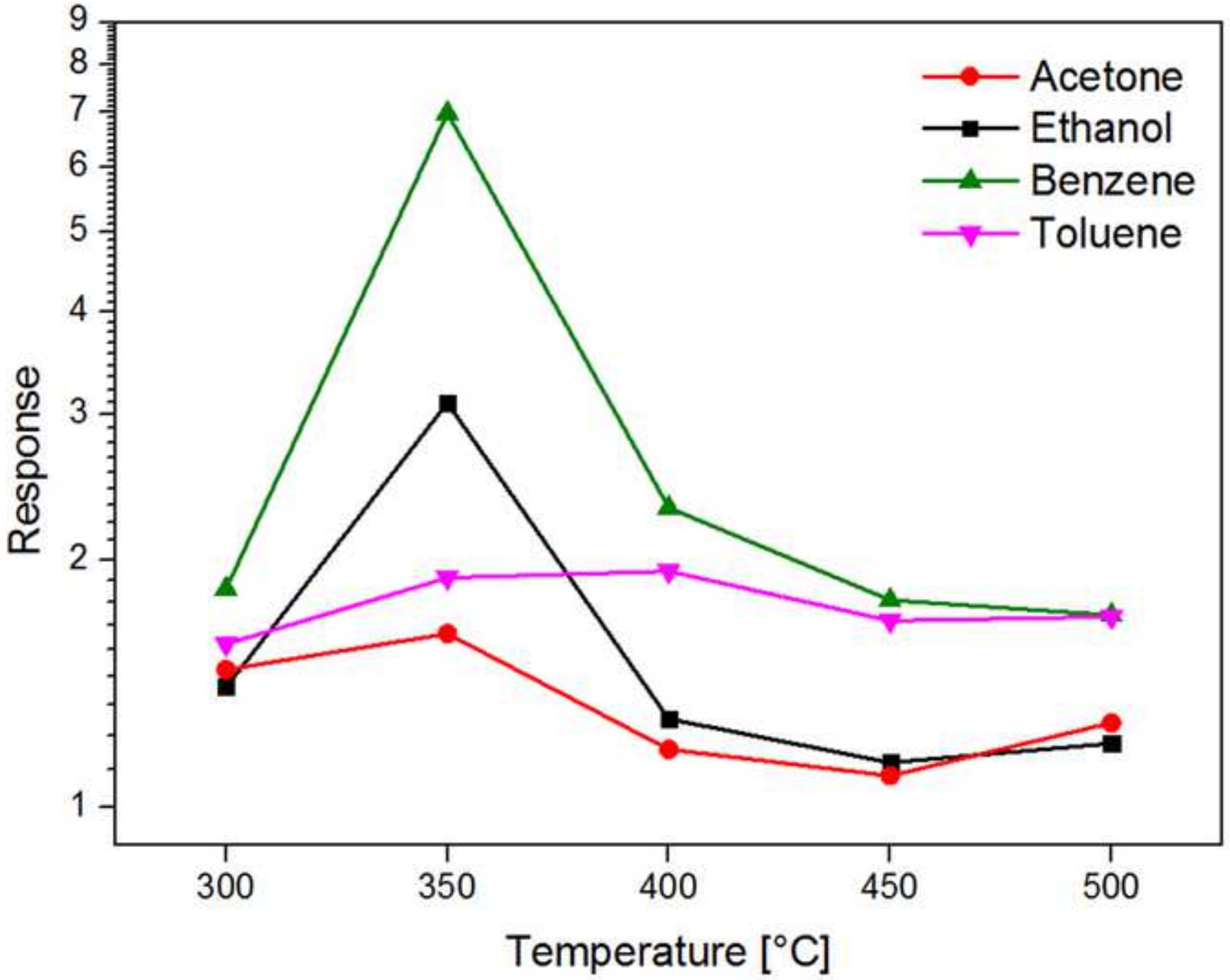

Figure 8

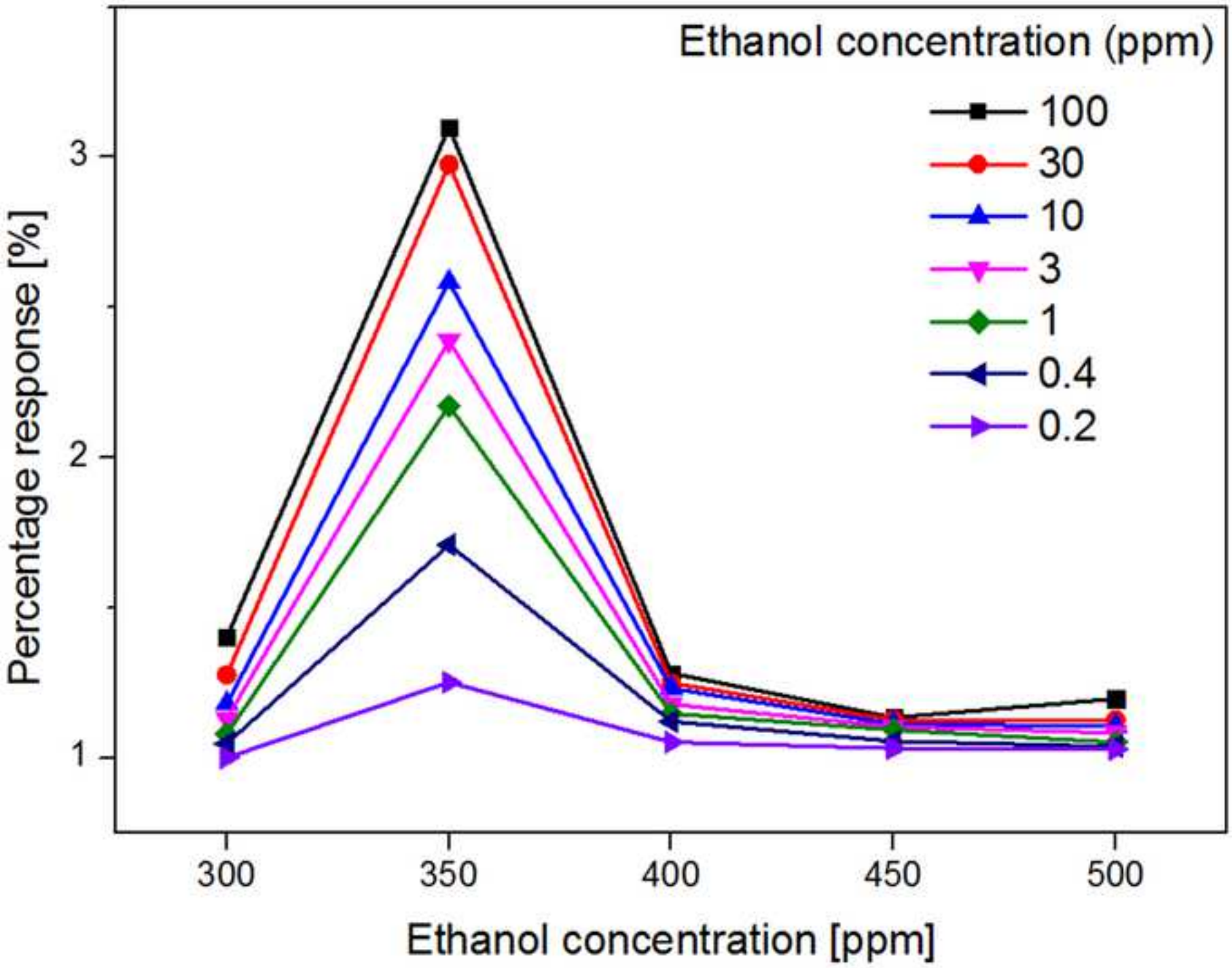

Figure 9

Click here to access/download;Figure(s);Fig. 9.tif

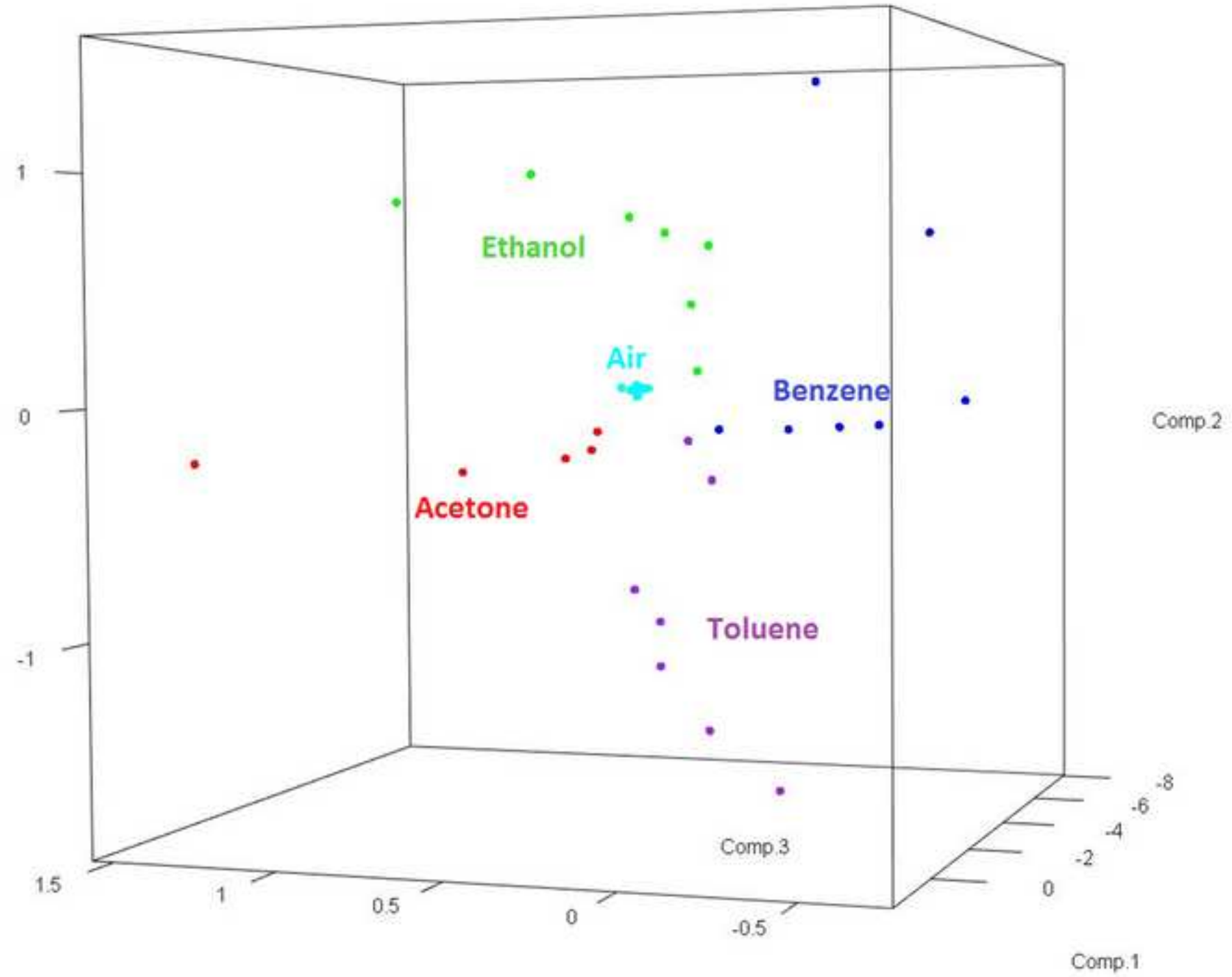

Figure 10

Click here to access/download;Figure(s);Fig. 10.tif

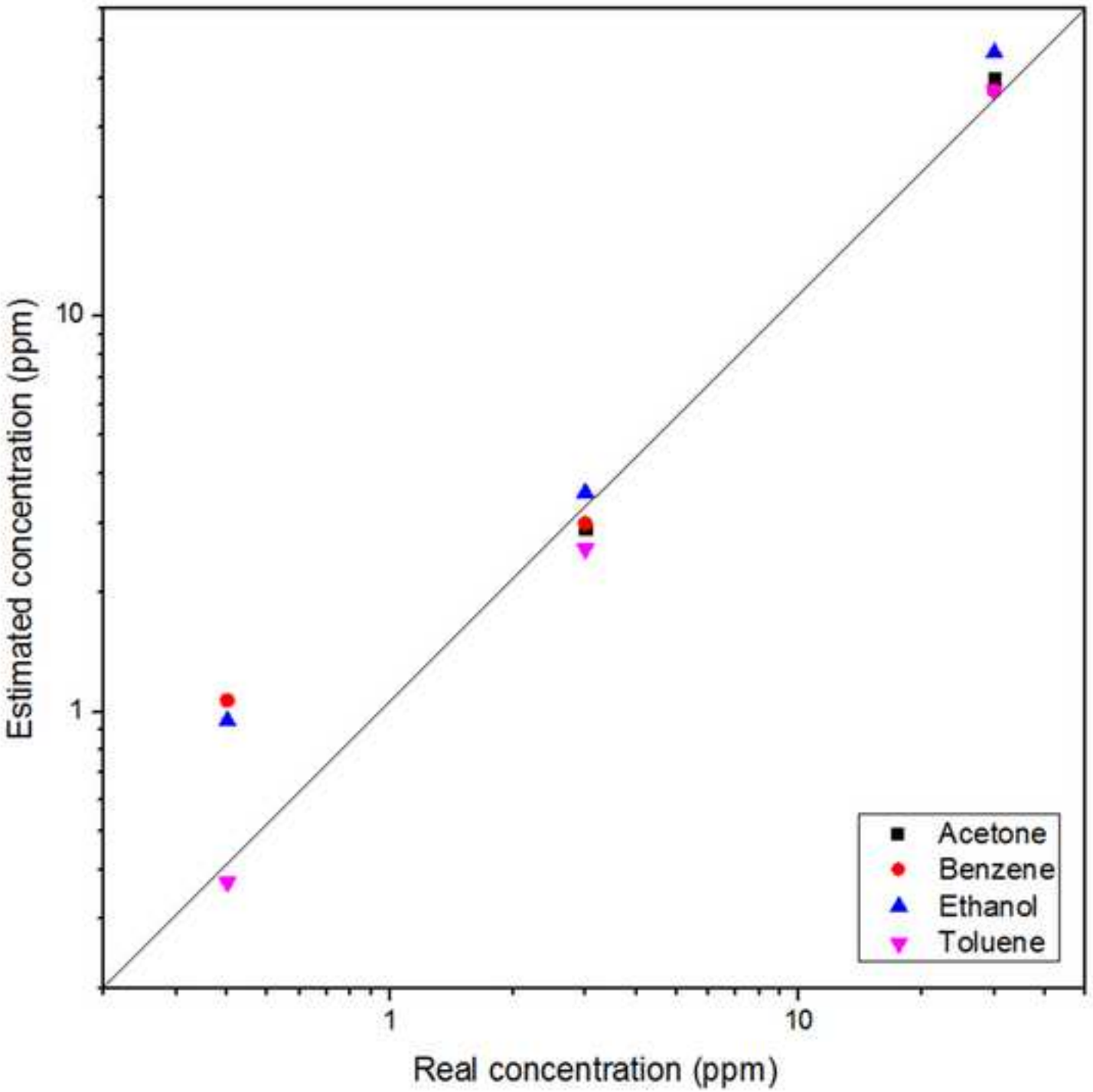

Biographies

Matteo Tonezzer graduated "cum laude" in Physics of the Matter and received his PhD degree "with honor" from the Faculty of Physics at the University of Trento, Italy, in 2011. In 2011, he won the Young Scientist Award from the European Materials Research Society (EMRS). He worked in research centers in France (ESRF), Brazil (UFMG), Vietnam (HUST), and USA (GaTech). He is currently working for IMEM at the Italian National Research Council. Major research interests are synthesis and characterization of nanostructured materials and their sensing properties.

Jin-Young Kim received his B.S. degree from Inha University, Republic of Korea in 2017. He is now working as a M. S. degree at Inha University, Republic of Korea. He has been working on oxide nanowire gas sensors.

Sang Sub Kim joined the Department of Materials Science and Engineering, Inha University, in 2007 as a full professor. He received his B.S. degree from Seoul National University and his M.S and Ph.D. degrees from Pohang University of Science and Technology (POSTECH) in Material Science and Engineering in 1987, 1990, and 1994, respectively. He was a visiting researcher at the National Research in Inorganic Materials (currently NIMS), Japan for 2 years each in 1995 and in 2000. In 2006, he was a visiting professor at Department of Chemistry, University of Alberta, Canada. In 2010, he also served as a cooperative professor at Nagaoka University of Technology, Japan. His research interests include the synthesis and applications of nanomaterials such as nanowires and nanofibers, functional thin films, and surface and interfacial characterizations.

Declaration of interests

☒ The authors declare that they have no known competing financial interests or personal relationships that could have appeared to influence the work reported in this paper.

☐The authors declare the following financial interests/personal relationships which may be considered as potential competing interests:

Sincerely Yours

Matteo Tonezzer, Ph.D.
Senior Researcher
IMEM-CNR
sede di Trento - FBK, Via alla Cascata 56/C, Povo (TN)
Italy

Sang Sub Kim, Ph.D.
Professor
Department of Materials Science and Engineering
Inha University
Incheon, 22212
Republic of Korea

CRediT author statement

Jin-Young Kim: Sensing measurement, Visualization, Investigation.

Sang Sub Kim: Conceptualization, Methodology, Writing- Reviewing and Editing,

Supervision

Matteo Tonezzer: Visualization, Investigation. Software, Writing- Original draft preparation.

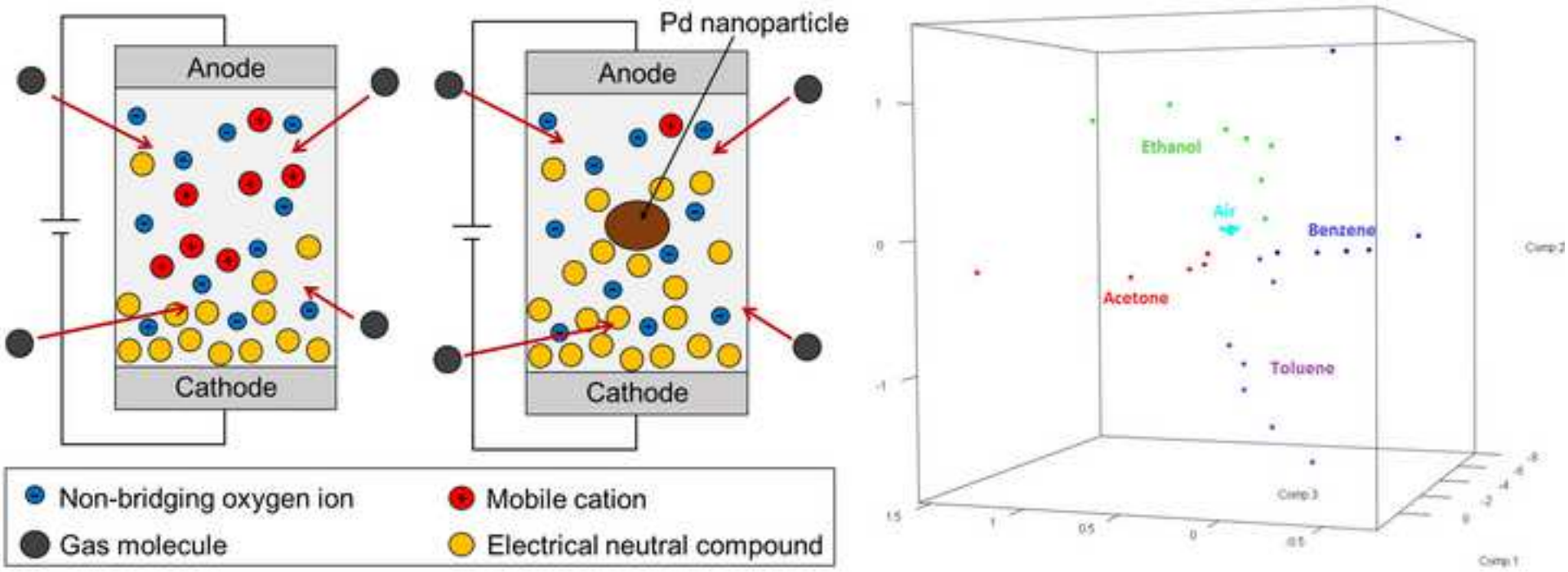

Selective gas detection and quantification using a resistive sensor based on Pd-decorated soda-lime glass

Jin-Young Kim[a], Sang Sub Kim[a,*], Matteo Tonezzer[b,c,d, *]

[a] *Department of Materials Science and Engineering, Inha University, Incheon 22212, Republic of Korea*

[b] *IMEM-CNR, sede di Trento - FBK, Via alla Cascata 56/C, Povo (TN), Italy*

[c] *University of Trento, Via Calepina 14, Trento, Italy*

[d] *Department of Food Quality and Nutrition, Research and Innovation Centre, Fondazione Edmund Mach (FEM), San Michele all' Adige (TN), Italy*

[*] Corresponding authors.

E-mail addresses: sangsub@inha.ac.kr (S.S. Kim), matteo.tonezzer@cnr.it (M. Tonezzer).

ABSTRACT

A commercial soda-lime glass slide was decorated with palladium nanoparticles by UV light irradiation. The response, limit of detection, response and recovery times of the resistive gas sensor obtained were investigated at different temperatures (300-500°C) with four different gases (acetone, benzene, ethanol, and toluene). To overcome the main problem of this type of sensor (the lack of selectivity due to the one-dimensional output signal) a new approach was applied, which merges the sensor response values at different working temperatures. The responses obtained at five different temperatures (300-500°C), combined into 5-dimensional points, were then analyzed using a support vector machine. After a calibration with a training dataset, the detection system was able to accurately classify (recognize the gas) and quantify (estimate its concentration) all tested gases. The results showed that this sensing system achieved perfect classification (100%) and a good estimation of the concentration of tested gases (average error <19% in the range 1-30 ppm). These performance demonstrate that with our approach (different temperatures and machine learning) a single resistive sensor made of glass can achieve true selectivity and good quantification, while remaining much simpler, smaller and cheaper than an electronic nose.

Keywords: Gas sensor, Soda-lime glass, Pd, Selectivity, Machine learning

1. Introduction

The detection of volatile compounds and gases in different places (work, home, car interiors, hospitals, etc.) is increasingly important because of the pollution related to urbanization and industrialization. A capillary network of sensors is important in agriculture [1], food and beverage quality control [2], security against terrorism [3], and medical diagnosis [4].

Metal oxide semiconductors (MOS) are being used extensively as gas sensors because of their high sensitivity to a wide range of gases and compounds and relatively simple detection mechanism, providing an easily processable signal. MOS nanostructures are the last and best generation of such devices because their huge surface-to-volume ratio gives them a very high active interface with gas particles, thereby increasing their response [5]. In addition, the properties of the sensors can be tuned by changing the size and shape of MOS nanostructures because of their structure-dependent behavior [6,7]. Unfortunately, the stability of these nanostructures to temperature and humidity requires improvement. Different approaches, such as hybrid nanostructures [8,9] and surface decoration with catalytic noble metal nanoparticles, have been used to improve the sensitivity and selectivity of MOS gas sensors [10,11]. Metal nanoparticles work through two effects: chemical and electronic sensitization. In the first case, the metal has catalytic activity that depends on the gas being detected, as well as its dissociation and adsorption. In the second case, a Schottky barrier is formed at the interface between the two materials, and the modulation of its height greatly improves the sensor response.

Most substrates used for such devices are silicon or glass [12,13]. Recently, glass has also been investigated as a sensing material because it is inexpensive and can be worked easily with microelectronics techniques. This way, the glass can act as both the structural substrate and active sensing material. Porous glass was impregnated through two-step coloration reactions to obtain an optical sensor that can detect ppb-levels of NO_2 [14]. A thin film of fast

proton-conducting glass was used to fabricate solid-state potentiometric hydrogen and methanol sensors that can work at room temperature [15,16]. Peres et al. used glass material as a resistive sensor for the first time in 2018, demonstrating its ability to discriminate different VOC vapors [17]. The sensing mechanism of soda-lime glass was recently investigated. The results showed that the glass polarization is affected by the reaction of gaseous species on its surface [18]. Because the diffusion of ions inside the glass is a thermally activated effect, the sensing performance is expected to change with working temperature. A recent study focused on the functionalization of soda-lime glass with different noble metal nanoparticles to compare their sensing performance [19].

Unfortunately, the main problem with this type of sensor whose output signal is one-dimensional (for example current or voltage) is that the response is a pure number, and therefore inherently non-selective. For this reason, a resistive sensor works well only in limited conditions, when the gas to be measured is only one. To overcome this defect, numerous sensors based on different materials are often used together in an array, in order to increase the dimensionality and therefore the information that the sensing system gives out [20,21]. This is the approach used in *electronic noses*, which have attracted considerable interest [22-24]. Unfortunately, this traditional approach in electronic noses requires separate electrical connections for each sensor and different conditions for each material (metal oxides need high temperatures, polymers and small conjugated molecules need low temperatures, etc.) and this makes them complex, large, and expensive.

Therefore, a different approach was used in this study to achieve true selectivity while keeping the complexity and size of the device low: different temperatures were used instead of different materials [25,26]. In this novel approach, the responses obtained at different working temperatures were combined (similar to how the responses from different materials are combined in traditional electronic noses), and processed through machine learning algorithms [27,28].

Specifically, in this study a single slide of soda-lime glass was functionalized with Pd nanoparticles and used at the same time as a substrate and sensing material between interdigitated metal electrodes. The sensor responses at different temperatures (300–500°C) were combined in a more informative five-dimensional 5D output that was processed using a machine-learning algorithm (support vector machine, SVM). Each 5D point was the combination of five responses at the same concentration of the same gas, but collected at different working temperatures. A first dataset of 5D points was used to train the system (a kind of calibration), while a second dataset of 5D data was used to test the sensor performance.

The detection system obtained a perfect classification (accuracy and specificity = 100%) of the four tested gases (acetone, benzene, ethanol and toluene) and a good estimate of their concentrations (error <19% for concentrations above 1 ppm). These results demonstrate that by exploiting the response at different temperatures, real selectivity can be achieved using only a simple soda-lime glass based resistive sensor.

2. Experimental

2.1. Preparation of the Pd-functionalized soda-lime glass

Soda-lime glass microscope slides were purchased from Knittel-Gläser (Germany). The soda-lime glass surface was functionalized by dipping the slides into a solution of $PdCl_2$ dissolved in deionized water (Fig. 1b). The glass slides were then irradiated with 0.11 mW/cm^2 of UV light for 1 s (Fig. 1c). The short irradiation time (like the choice of Pd functionalization) was determined from an optimization step recently reported [19]. Finally, to remove residual solvents and improve the crystallization of the Pd nanoparticles functionalized on soda-lime glass slides, the samples were annealed at 500°C for 30 min (Fig. 1d). The sensing material was ready at the end of these steps (Fig. 1e).

2.2. Characterization

The morphology of the functionalized glasses was examined by field emission scanning electron microscopy (FE-SEM, JEOL 7600 F). The elemental composition of the Pd-glass slide was investigated by energy-dispersive X-ray spectroscopy (EDX) incorporated in the FE-SEM. The hysteresis I-V loops were measured using a Keithley 2400 sourcemeter.

2.3. Gas sensing test

The gas sensor was fabricated by depositing interdigitated electrodes (Pt over Ti, with a thickness of 200 and 50 nm, respectively) by DC sputtering on the glass surface through shadow masks (Fig. 1f,g). The two comb-like electrodes had seven fingers with a width of 400 microns and a gap of 400 microns between them (Fig. 1h,i). The two metal electrodes were connected to a Keithley 2400 Sourcemeter, and a constant DC bias of 1 V was applied. The current flowing through the sensing material was used to calculate the dynamic response of the sensor. The sensor was then inserted into a horizontal-quartz oven that could be heated to several hundred degrees Celsius. Pure synthetic dry air was flowed into the chamber for 30 min while the sensor was kept at a constant DC bias of 1 V to stabilize its signal. Each target gas (acetone, benzene, ethanol, and toluene) was then injected cyclically into the sensing chamber, while maintaining a total flow rate of 500 sccm. The sensor response was calculated as I_g/I_a, where I_g is the current in the presence of a target gas, and I_a is the current flowing through the sensor in dry air.

3. Results and discussion

3.1. Characterization of the Pd-functionalized glass

The morphology of the glass slide before and after the functionalization with Pd nanoparticles was examined by FE-SEM, as shown in Fig. 2. Several Pd nanoparticles covered the glass surface homogeneously (Fig. 2b), which is in contrast to the smooth surface

of the bare glass shown in Fig. 2a. The particles had diameters in the range of 100–200 nm. This coverage was chosen because a previous study found it to be the most effective for improving the sensing properties of soda-lime glass [19]. EDX was carried out to confirm the chemical composition of the nanoparticles. Figs. 2c and d present the EDX spectra of the bare and Pd-functionalized glass samples, respectively. The evident peaks corresponding to Si, O, Na, Ca, Mg, and Al indicate that the samples are typical soda-lime glass. A peak from Pd was observed only for the Pd-functionalized sample, as shown in Fig. 2d, showing that the nanoparticles formed on the bare glass slide were Pd. Table S1 lists the chemical composition estimated from the integration area of a peak in the EDX spectra. The observed morphology and chemical composition confirmed that the functionalization process of the surface was successful.

3.2. Sensing mechanism of the Pd-functionalized glass

The electrical properties of the Pd-functionalized soda-lime glass sensor were investigated to understand the sensing mechanism. The results show that the sensor had significant electrical conductivities at high temperatures, as shown in Fig. 3. The hysteresis feature of the soda-lime glass sample appeared only at 300^{o}C, as shown in Fig. 3a. In addition, the maximum current during the I-V loops depends strongly on the sweeping speed, while showing a similar shape for various voltages at the same sweeping speed, as shown in Fig. 3b. This behavior indicates the accumulation of electrostatic surface charges by local electrochemical effects between the electrodes under bias [29,30].

Exponential capacitive decay was observed upon DC biasing (Fig. 3c), indicating that polarization developed in the Pd-functionalized soda-lime glass [31-33]. The three continuous runs took 30 minutes to reach a steady current of approximately 0.045 μA at 300°C and 1 V DC bias. At this stage, the maximum charge was stored between the electrodes by glass polarization [34,35]. The electrical charge eventually dissipates during a final continuous run,

i.e., 0 V-4th run in Fig. 3c. A significant negative current, ranging from -0.37 to -0.03 μA, flowed through the sourcemeter without an external bias for more than 500 s after the three continuous runs, eventually leading to an equilibrium zero current. The temperature-dependent hysteresis I-V loops (Fig. 3d) revealed the Arrhenius behavior [36] of the conductivity in the Pd-functionalized soda-lime glass sample. In our earlier report [18], the I-V characteristics of bare soda-lime glass were presented. For example, the I–V loop obtained at 1 V and sweeping rate of 120 s/sweep at 300^{o}C revealed a current of ±0.21 μA, corresponding to a resistance value of 4.76 MΩ. This confirms that the soda-lime glass without Pd decoration is quite insulating. The I-V loops obtained from the Pd-decorated soda-lime glass at the same condition revealed a current of ±0.12 μA, corresponding to a resistance value of 8.33 MΩ. This indicates that the Pd decoration makes a greater resistance value in comparison to the bare soda-lime glass.

A previous study described the gas sensing mechanism for the Pd-functionalized glass [19]. Under high working temperatures, alkali ions with a positive charge in the soda-lime glass can gain good mobility and rearrange themselves under an applied external electric field. This results in a concentration gradient of the cations, leading to the macroscopic glass polarization, as shown schematically in Fig. 4a. Under this circumstance, the output current (I) at a fixed applied voltage can be explained as $I=I_v-I_c$, where I_v and I_c are voltage- and charge-dependent current terms, respectively. Although I_v is dependent only on the applied voltage, I_c is strongly dependent on the number of mobile cations. When a bias voltage is applied, mobile alkaline positive ions, such as Na^+, are highly populated near the cathode. Electrical neutral compounds (ENCs) were formed when a target gas was introduced to the glass sensor, reducing the polarization of the glass sensor. Accordingly, I_c decreases, which can explain the increase in total current when a target gas is introduced.

As illustrated in Fig. 4b, Pd nanoparticles can play a catalytic role in facilitating the

decomposition of target gas molecules and providing a spillover effect, leading to more surface reactions. Hence, more ENCs were generated, and I_c is reduced further. This is why Pd functionalization gives an increased output current, resulting in an enhanced gas response. In our earlier work [19], the specific effects of metal decoration such as Pd, Pt and Au on soda-lime glass were investigated. The gas sensing results revealed that Pd functionalization leads to a relatively high selectivity to benzene. This selective sensing property was explained by the adsorption energy of benzene onto Pd. The experimental adsorption energy of benzene onto Pd was 1.35 eV, which is a good value for easy adsorption and desorption in comparison with the values of other metals.

As shown in Fig. S2, sensing properties toward hydrogen and ammonia gases of the Pd-decorated soda-lime glass sensor were also tested. Regardless of the well-known effect of Pd on hydrogen sensing capability, the sensor in this work showed a superior benzene-sensing capability in comparison with all other tested gases such as ethanol, acetone, toluene, hydrogen, and ammonia at the optimized operating temperature of 350^{o}C.

3.3. Dynamic current and traditional selectivity

The Pd-functionalized glass sensor was exposed to different concentrations of acetone, benzene, ethanol, and toluene gas, as listed in Table S2. The background color of the columns will be important in the next section, when it will be used to explain the machine learning post-processing.

As a first step, the dynamic current passing through the sensor was measured during a few gas cycles at different concentrations. All the plots showed similar behavior (Fig. 5), with the dynamic current increasing steeply when the gas was injected and then decreasing when the gas was expelled. The current increased significantly with increasing gas concentration. In all cases, the current returned to its previous value, proving the reversibility of the sensor response. During each peak (a period in which the gas concentration was constant), the sensor

current tended to drop more or less noticeably. This did not affect the sensor operation because the decrease was slow compared to the sensor response and recovery times.

The sensor responses for each gas were calculated from Fig. 5, as described in Section 2.3. Fig. 6 presents the results for 100 ppm for each gas. Typically, these measurements are used to determine the optimal working temperature for a sensor to maximize its response. In the present case, these data are much more important. The responses towards all gases reached their maximum at the same temperature: 350°C. The sensor stability was tested by measuring the dynamic sensing curve for repeated cycles of 10 ppm benzene gas at 350°C, and the result is shown in Fig. S1. It shows that the sensor responses fall in a reasonable error range for five measurements, evidently demonstrating the good sensor stability. More important than the temperature at which the maximum response is obtained, is the internal structure between the bars at 350°C, showing that the selectivity also reached its maximum at this temperature. Note that the selectivity is traditionally defined as the lowest value among the partial selectivities, which were calculated on each couple of gases [37]. For example, at all temperatures the sensor was selective to benzene, with toluene being the first interferer (except at 350°C). At 350°C, the responses of both ethanol and benzene increased considerably; the sensor was still selective to benzene, but the first interferer, in this case, was ethanol. The selectivity of benzene towards the other interfering gases was as follows: 4.3 (acetone), 2.25 (ethanol), and 3.7 (toluene). Therefore, the overall selectivity of the sensor at 350°C was 2.25. The selectivity was calculated at different temperatures to confirm the best selectivity of the sensor, as listed in Table 1.

The selectivity at 350°C was the best for the glass sensor, which showed more than double the response to benzene than to ethanol. A situation like the one in Fig. 2 at 350°C was much better than that at 300°C because the sensor responds much more intensely to a single gas than to the other gases.

Nevertheless, if one of the tested gases is injected on the sensor without knowing which

one, there is no information as to which gas it is. Any response could be generated by a low concentration of benzene, a higher concentration of ethanol, or an even higher concentration of acetone or toluene. Therefore, a novel approach was applied, which uses the response values at different working temperatures as multidimensional data to be processed by machine learning algorithms to achieve real selectivity. This idea combines the different responses (obtained at different working temperatures) in more informative 5D points.

Each very informative 5D point contains the five response values and all the correlations among them. In other words, each 5D point summarizes one *thermal fingerprint* (response as a function of the working temperature), as shown in Fig. 7, and previously explained elsewhere [38,39].

Each plot in Fig. 7 is relative to one gas and can be used to recognize it with future measurements because its shape is characteristic of that gas. In a first step, a series of these fingerprints (in form of 5D points) was given to the sensing system to teach it how to recognize each gas (like a more complex calibration step). During this step, a set of 5D points was provided with two labels: the name of the gas and its concentration. The sensing system can learn the shape of each gas-specific fingerprint, and, by comparing the fingerprint of a new unknown measurement, recognize the gas in a new test. The second label (the gas concentration) is important because the fingerprint of each gas maintains the same shape, but changes with the gas concentration, as shown in Fig. 8.

Fig. 8 shows the thermal fingerprints obtained for different concentrations of ethanol gas. The shape of the fingerprint remains the same, but the intensity increases with increasing gas concentration. Owing to these two labels, the system can learn how to recognize each gas and subsequently estimate its concentration. Note that the system can be trained to recognize new gases and distinguish them. The system only needs a first training dataset for each gas, as for a simpler calibration step.

3.4. Principal component analysis (PCA)

Because the data used by the sensing system are 5-dimensional, it is impossible to visualize them on a screen or paper. To give the reader an idea of how the sensor works, a dimensions reduction was applied through principal components analysis (PCA). This unsupervised method is a statistical procedure, in which the data are fed to the system with no label. The procedure is used frequently to reduce the number of dimensions and allow the data to be visualized. This type of projection chooses the principal components as the orthogonal directions, maximizing the variance of each subsequent component.

Fig. 8 shows the first three principal components, helping to visualize the relationships among the points better. Each point in Fig. 9 is the reduction from a 5D point to a 3D point, which contains all the measurements of the same gas at the same concentration but at different working temperatures. Each segmented line in Fig. 7 or 8 is combined in a multidimensional point that is then minimized in a colored point in Fig. 9. Only the training points come with a label that identifies them as relating to a certain gas, which translates into a color in the PCA plot. A small dense cloud of cyan points, relative to air without any target gas, can be seen in the center of Fig. 9. The points cluster quite densely because there is no difference among them. Therefore, the different position rises only from the error on the raw signal from the sensor. Around this cyan cloud, the points relative to the target gases (acetone in red, ethanol in green, benzene in blue, and toluene in purple) lay on curved lines, quite far from each other. Owing to the PCA projection, they are well separated and easy to distinguish.

The fact that the points of each gas are not grouped in a small cloud (as is often reported) is not a weak point of this method. Points lying on lines instead of in small clouds make it more difficult to classify a system. However, this makes it possible to perform further analysis and obtain an estimate of the gas concentrations, as shown in section 3.6.

3.5. Classification of gases

As shown in the previous section, points relating to different gases occupy different regions of space. The points relating to the different gases are recognizable in Fig. 9, facilitating the classification of new unknown points based on their position with respect them. For example, a new gray dot from a new sensor measurement can be classified by looking at Fig. 9 and seeing near which line of dots it is placed. If it is close to the purple spots, the gas in question will likely be toluene. This assessment can be made using the human eye; however, the sensing system can work in five dimensions.

The core of the sensing discrimination and selectivity is a support vector machine, which is a supervised learning algorithm that produces a model consisting of 4D hyperplanes in 5D, which indicate the boundaries between 5D areas corresponding to different gases. This model is produced using a first dataset of training points (the ones shown in Fig. 9) to recognize the regions of 5D space "belonging" to each target gas.

Any new data (the points with a white background in Table S2) are compared by the system with the trained model to classify it. Table 2 lists the confusion matrix of the sensor classification; each row is related to the actual gas in the sensing chamber, while each column is giving the gas that the sensing system has identified. This means that the numbers on the diagonal of the matrix are correctly identified measurements, while those outside are misclassified. As listed in Table 2, the Pd-decorated soda-lime glass sensors performed perfect classification, with an accuracy and a specificity of 100%. This proves that the SVM, working in 5D space, discriminates even better than the human eye with only a three-dimensional plot in Fig. 9.

As shown in Fig. S3, the sensor was also tested with a 50-50% mixture of benzene and toluene, in order to verify if the system is able to distinguish and quantify even gas mixtures. As can be seen, the points relating to the two gases and the mixture are well separated, and follow distinct lines. It should be emphasized that the concentration, in all three cases, increases from bottom to top in the figure (from 1 to 100 ppm). The first step carried out by

the sensor is to distinguish the two gases and the mixture. A support vector machine acts as a classifier, and recognizes (using a first series of "calibration" points) the areas of the 5D space where the points relating to benzene, toluene and the mixture are located. In this way, each new measurement made with the sensor is automatically labeled by the system, which recognizes what is present in the measurement chamber, whether it is gas or mixture.

3.6. Estimation of gas concentration

The previous section showed that the sensing system can perfectly classify the test gases, even if the new measurements are taken at different concentrations. In other words, the sensor can distinguish the 5D space areas related to each gas, even if the points of each gas in Fig. 9 are very far from each other. This arrangement of points makes the classification more difficult, but it can achieve a further objective, which is illustrated and explained. Small and dense clouds of points from PCA plots (unlike in Fig. 9) can be managed easily using untrained methods, relying on the distance between points. On the other hand, this arrangement makes it impossible to differentiate the points belonging to the same gas at different concentrations.

Because the points in Fig. 9 are distant and positioned on lines, a support vector regressor can be used to estimate the gas concentration of each point [40,41]. This step must be done after the previous one because the system needs to know how the gas has been classified. As in the previous section, the classification occurs using four different combined dual classifiers; here, four regressors are used, one for each gas. Each SV regressor is trained with the data classified for that gas, using their concentration label. Each new point is sent to the regressor chosen by its classification. An incorrect classification would often lead to an incorrect estimate of the concentration.

The sensing system can understand which gas is present and its concentration, even though that gas has not been tested at that specific concentration. Fig. 10 presents the support

vector regression results, where each gas is plotted in a different color. As already mentioned, if a point is classified incorrectly in the previous step, it would be plotted with a different (incorrect) color.

The points in Fig. 10 indicate the regression results: the concentration estimate versus the real concentration of the gas. The true concentrations (on the abscissas) correspond to those of the test points (those with a white background in Table S2). The quality of the regressor estimates is easy to evaluate in Fig. 10 because the diagonal indicates the perfect estimate, which corresponds to the true concentration. As shown in Fig. 10, the points relative to all four gases are laying close to the diagonal, meaning that the estimated concentrations are good. The mean percentage error for each gas was calculated to quantify how good the concentration estimate is, as listed in Table 3.

The test points were chosen to be alternating with those used to teach the model, as listed in Table S2. In this way, the test points are as far as possible from the reference points, and the error is the maximum achievable. This means that measurements of random concentrations (a more realistic case) would be characterized by a smaller error. Benzene and ethanol showed larger errors than acetone and toluene. The sensor could not detect acetone at sub-ppm concentrations; thus, the point at 0.2 ppm is missing for acetone. The error was strongly affected by the points on the left (Fig. 9). Indeed, the error has a common trend for most gases; it is higher at low concentrations, lower in the middle, and larger (but less) at higher concentrations.

Two effects can explain this: i) the calibration border and ii) the proximity to the limit of detection [42]. The support vector machine model works like a calibration; it works worse away from trained concentrations. Hence, the model is weaker approaching the border of the trained interval, and the error is larger. This occurs at both extremities of the tested concentrations range. Furthermore, the limit of detection of the sensor is being approached on the left of Fig. 10. Therefore, the raw response of the resistive sensor gradually loses its

meaning. This second effect adds to the first, further enlarging the error of the estimate.

The analysis can be limited to this concentration interval, given that most of the hazard thresholds are in the ppm range. If the average percentage error leaving out the points below 1 ppm can be calculated, the sensing system is much more precise, as shown in Table 4. Considering only the concentrations above 1ppm, the average percentage errors are 13.2%, 29.4%, 18.2%, and 14.7% for acetone, benzene, ethanol, and toluene, respectively. In addition, as shown in Fig. S4, The error on the measurement of the mixture concentration (14.4%) is comparable to that made on the single gases (benzene 13.3%, toluene 8.5%). Such errors are acceptable, especially considering that the dangerousness of the various gases varies with the order of magnitude of the concentration and not with the individual ppm.

These results indicate that this is not a theoretical technique, because it has proven to be able to discriminate individual gases perfectly (100% correct classification) in the case of real measurements, even in double blind conditions. It is also worth pointing out that with this technique the sensor system makes decisions autonomously, without the need for the presence of a human operator.

4. Conclusions

A resistive gas sensor based on Pd-decorated soda-lime glass with metal interdigitated electrodes was fabricated and used to detect four different reducing gases (acetone, benzene, ethanol, and toluene). The response values obtained at five different working temperatures (300-500°C in steps of 50°C) were combined in highly informative 5-dimensional points, which were then processed using machine learning algorithms. Using a support vector machine as a classifier and then as a regressor, one single sensor was able to discriminate all four gases perfectly (100%) and estimate their concentrations with an average error <19%. With this novel approach that uses one single sensor at different temperatures instead of several sensors of different materials, it was possible to achieve true selectivity and good

quantification with a much smaller, simpler and cheaper detection system than a traditional electronic nose. This could allow the widespread diffusion of tiny selective sensors integrated into portable devices and networked, enabling to monitor the environment much more effectively.

Acknowledgments

This study was supported by Inha University and the Institute of Materials for Electronics and Magnetism (IMEM-CNR).

Appendix A. Supplementary data

Supplementary data associated with this article can be found in the online version at http://dx.doi.org/

References

[1] A.A. Makky, A. Alaswad, D. Gibson, A.G. Olabi, Renewable energy scenario and environmental aspects of soil emission measurements, Renewable Sustainable Energy Rev. 68 (2017) 1157–1173.

[2] D. Barreca, A. Gasparotto, F. Gri, E. Comini, C. Maccato, Plasma-assisted growth of β–MnO_2 nanosystems as gas sensors for safety and food industry applications, Adv. Mater. Interfaces 5 (2018) 1800792.

[3] Y. Ge, Z. Wei, Y. Li, J. Qu, B. Zu, X. Dou, Highly sensitive and rapid chemiresistive sensor towards trace nitro-explosive vapors based on oxygen vacancy-rich and defective crystallized In-doped ZnO, Sens. Actuators B Chem. 244 (2017) 983–991.

[4] M. Righettoni, A. Amann, S.E. Pratsinis, Breath analysis by nanostructured metal oxides as chemo-resistive gas sensors, Mater. Today 18 (2015) 163-171.

[5] A. Mirzaei, S.S. Kim, H.W. Kim, Resistance-based H_2S gas sensors using metal oxide nanostructures: A review of recent advances, J. Hazard. Mater. 357 (2018) 314–331.

[6] B.-Y. Wang, D.-S. Lim, Y.-J. Oh, CO gas detection of Al-doped ZnO nanostructures with various shapes, Jpn. J. Appl. Phys. 52 (2013) 101103.

[7] M. Tonezzer, T.T.L. Dang, N. Bazzanella, V.H. Nguyen, S. Iannotta, Comparative gas-sensing performance of 1D and 2D ZnO nanostructures, Sens. Actuators B Chem. 220 (2015) 1152–1160.

[8] I.S. Jeon, G. Bae, M. Jang, W. Song, S. Myung, S.S. Lee, H.-K. Jung, J. Hwang, K.-S. An, A synergistic combination of zinc oxide nanowires array with dual-functional zeolitic imidazolate framework-8 for hybrid nanomaterials-based gas sensors, Compos. B. Eng. 180 (2020) 107552.

[9] J. Hu, M. Chen, Q. Rong, Y. Zhang, H. Wang, D. Zhang, X. Zhao, S. Zhou, B. Zi, J. Zhao, J. Zhang, Z. Zhu, Q. Liu, Formaldehyde sensing performance of reduced graphene oxide-wrapped hollow SnO_2 nanospheres composites, Sens. Actuators B Chem. 307 (2020) 127584.

[10] J.-H. Lee, A. Mirzaei, J.-Y. Kim, J.-H. Kim, H.W. Kim, S.S. Kim, Optimization of the surface coverage of metal nanoparticles on nanowires gas sensors to achieve the optimal sensing performance, Sens. Actuators B Chem. 302 (2020) 127196.

[11] A. Katoch, S.-W. Choi, G.-J. Sun, S.S. Kim, Low temperature sensing properties of Pt nanoparticle-functionalized networked ZnO nanowires, J. Nanosci. Nanotechnol. 15 (2015) 330-333.

[12] V.V. Petrov, A.P. Starnikova, Y.N. Varzarev, K.A. Abdullin, D.P. Makarenko, Gas sensitive properties of ZnO nanorods formed on silicon and glass substrates, IOP Conf. Ser., Mater. Sci. Eng. 703 (2019) 012038.

[13] R. Prajesh, V. Goyal, V. Saini, J. Bhargava, A. Sharma, A. Agarwal, Development and reliability analysis of micro gas sensor platform on glass substrate, Microsyst. Technol.

25 (2019) 3589-3597.

[14] T. Tanaka, A. Guilleux, T. Ohyama, Y.Y. Maruo, T. Hayashi, A ppb-level NO_2 gas sensor using coloration reactions in porous glass, Sens. Actuators B Chem. 56 (1999) 247–253.

[15] M. Nogami, M. Matsumura, Y. Daiko, Hydrogen sensor prepared using fast proton-conducting glass films, Sens. Actuators B Chem. 120 (2006) 266–269.

[16] M. Nogami, T. Maeda, T. Uma, A methanol gas sensor based on inorganic glass thin films, Sens. Actuators B Chem. 137 (2009) 603–607.

[17] H.E.M. Peres, E. Galeazzo, M.O.S. Dantas, W. Beccaro, G.P. Filbrich, F.J. Ramirez-Fernandez, Evaluation of the electrical resistance response of insulating glass surface to sense and classify humidity and VOCs vapors, IEEE Sens. J. 18 (2018) 3940-3945.

[18] K.V. Sopiha, J.-H. Kim, S.S. Kim, P. Wu, Gas sensing properties of standard soda-lime glass, Sens. Actuators B Chem. 266 (2018) 344–353.

[19] J.-Y. Kim, A. Mirzaei, J.-H. Kim, J.-H. Lee, H.W. Kim, S.S. Kim, Incorporation of metal nanoparticles in soda-lime glass sensors for enhancing selective sensing, Sens. Actuators B Chem. 296 (2019) 126673.

[20] C.S. Prajapati, S. Benedict, N. Bhat, An ultralow power nanosensor array for selective detection of air pollutants, Nanotechnol. 31 (2019) 025301.

[21] S. Khaldi, Z. Dibi, Neural network technique for electronic nose based on high sensitivity sensors array, Sens. Imaging 20 (2019) 15.

[22] E.N. Carmona, V. Sberveglieri, A. Ponzoni, V. Galstyan, D. Zappa, A. Pulvirenti, E. Comini, Detection of food and skin pathogen microbiota by means of an electronic nose based on metal oxide chemiresistors, Sens. Actuators B Chem. 238 (2017) 1224–1230.

[23] H.G. Moon, Y. Jung, S.D. Han, Y.-S. Shim, B. Shin, T. Lee, J.-S. Kim, S. Lee, S.C. Jun, H.-H. Park, C. Kim, C.-Y. Kang, Chemiresistive electronic nose toward detection of biomarkers in exhaled breath, ACS Appl. Mater. Interfaces 8 (2016) 20969-20976.

[24] S. Jiang, J. Wang, Y. Wang, S. Cheng, A novel framework for analyzing MOS E-nose data based on voting theory: Application to evaluate the internal quality of Chinese pecans, Sens. Actuators B Chem. 242 (2017) 511–521.

[25] M. Tonezzer, D.T.T. Le, T.Q. Huy, S. Iannotta, Dual-selective hydrogen and ethanol sensor for steam reforming systems, Sens. Actuators B Chem. 236 (2016) 1011–1019.

[26] M. Tonezzer, Selective gas sensor based on one single SnO_2 nanowire, Sens. Actuators B Chem. 288 (2019) 53-59.

[27] T.M. Ngoc, N.V. Duy, C.M. Hung, N.D. Hoa, H. Nguyen, M. Tonezzer, N.V. Hieu, Self-heated Ag-decorated SnO_2 nanowires with low power consumption used as a predictive virtual multisensor for H_2S-selective sensing, Anal. Chim. Acta 1069 (2019) 108-116.

[28] M. Tonezzer, L.T.T. Dang, H.Q. Tran, S. Iannotta, Multiselective visual gas sensor using nickel oxide nanowires as chemiresistor, Sens. Actuators B Chem. 255 (2018) 2785–2793.

[29] R. Proksch, Electrochemical strain microscopy of silica glasses, J. Appl. Phys. 116 (2014) 066804.

[30] R.K. Vasudevan, N. Balke, P. Maksymovych, S. Jesse, S.V. Kalinin, Ferroelectric or non-ferroelectric: Why so many materials exhibit “ferroelectricity” on the nanoscale, Appl. Phys. Rev. 4 (2017) 021302.

[31] A. Wikby, G. Johansson, The resistance and intrinsic time constant of glass electrodes, J. Electroanal. Chem. Interf. Electrochem. 23 (1969) 23-40.

[32] K. Tamamoto, H. Namikawa, Conduction current relaxation of inhomogeneous conductor I, Jpn. J. Appl. Phys. 27 (1988) 1845.

[33] R.J. Charles, Polarization and diffusion in a silicate glass, J. Appl. Phys. 32 (1961) 1115-1126.

[34] A. Doi, Alkali motion in alkali silicate glass, J. Appl. Phys. 50 (1979) 1291-1297.

[35] C. McLaren, B. Roling, R. Raj, H. Jain, Mechanism of electric field-induced softening (EFIS) of alkali silicate glasses, J. Non Cryst. Solids 471 (2017) 384-395.

[36] H. Mehrer, Diffusion in Solids: Fundamentals, Methods, Materials, Diffusion-controlled Processes, Springer Science & Business Media, New York, 2007.

[37] W. Göpel, K.D. Schierbaum, Sensors: A comprehensive survey (City Publishers), vol. 2, VCH Publishers, New York, 1991.

[38] M. Tonezzer, T.T.L. Dang, Q.H. Tran, V.H. Nguyen, S. Iannotta, Selective hydrogen sensor for liquefied petroleum gas steam reforming fuel cell systems, Int. J. Hydrog. Energy 42 (2017) 740-748.

[39] M. Tonezzer, J.-H. Kim, J.-H. Lee, S. Iannotta, S.S. Kim, Predictive gas sensor based on thermal fingerprints from Pt-SnO_2 nanowires, Sens. Actuators B Chem. 281 (2019) 670-678.

[40] S. Xu, X. An, X. Qiao, L. Zhu, L. Li, Multi-output least-squares support vector regression machines, Pattern Recognit. Lett. 34 (2013) 1078–1084.

[41] M. Tonezzer, D.T.T. Le, S. Iannotta, N.V. Hieu, Selective discrimination of hazardous gases using one single metal oxide resistive sensor, Sens. Actuators B Chem. 277 (2018) 121-128.

[42] M. Tonezzer, S.C. Izidoro, J.P.A. Moraes, L.T.T. Dang, Improved gas selectivity based on carbon modified SnO_2 nanowires, Front. Mater. 6:277. https://doi.org/10.3389/fmats.2019.00277.

Table and Figure Captions

Table 1. Selectivity measured at different working temperatures.

Table 2. Confusion matrix for the testing points (in each row, there is the true gas, while in each column, there is the gas identified by the sensing system).

Table 3. Average percentage error calculated for each gas.

Table 4. Average percentage error calculated for each gas, limited to concentrations greater than 1 ppm.

Fig. 1. Process steps to obtain the sensing material (a-e) and steps to fabricate the sensing device (f-i). (a) Commercial soda-lime slide, b) immersion in solution, c) irradiation with UV light, d) annealing at 500°C, e) Pd-functionalized soda-lime glass. f) deposition of an adhesion layer of Ti, g) deposition of the Pt electrode, h) final sensor, i) cross-section of the sensor to show the different materials.

Fig. 2. FE-SEM images and EDX spectra of the bare glass (a and c) and Pd-functionalized glass (b and d) surfaces, respectively.

Fig. 3. Electrical characteristics of the Pd-functionalized soda-lime glass: (a) Normalized hysteresis I-V loops using at different temperatures in a continuous sequence from 100 to 300^{o}C with 120 s/sweep sweeping speed. (b) Hysteresis I-V loops for various sweeping speeds measured in a continuous sequence from 12 to 120 s/sweep at 300^{o}C. The inset presents the hysteresis I-V loops obtained at various sweeping voltages in a continuous sequence from 0.5 to 5 V using sweeping speed for 120 s/sweep at 300^{o}C. (c) Capacitive decays of current obtained under 1 V DC bias for three continuous runs, followed by the fourth unbiased run at 300^{o}C. (d) Temperature dependence of the electrical conductance. The data points represent the corresponding conductance values calculated with the current I values during the I-V sweeping at various temperatures.

Fig. 4. Schematic illustration of the sensing mechanism of Pd-functionalized soda-lime glass: (a) Macroscopic glass polarization under external electric field and cation change by the target gas in a bare glass. (b) Catalytic effect by Pd functionalization after the introduction of the target gas.

Fig. 5. Plots of the dynamic current measured at different temperatures for different gases at

different concentrations.

Fig. 6. Sensor response to 100 ppm of each gas, measured at different temperatures.

Fig. 7. Thermal fingerprints (sensor response as a function of working temperature) relative to each gas, measured at a concentration of 100 ppm.

Fig. 8. Thermal fingerprints (sensor response as a function of the working temperature) relative to different concentrations of ethanol gas.

Fig. 9. Three-dimensional plot of the first three principal components, showing the data relative to the different gases in different colors.

Fig. 10. Concentration estimate by the sensing system (Y-axis) versus real concentration (X-axis). Perfect estimates lay on the diagonal.

Table 1. Selectivity measured at different working temperatures.

Temperature	300°C	350°C	400°C	450°C	500°C
Target gas	benzene	benzene	benzene	benzene	benzene
First interferer	toluene	ethanol	toluene	toluene	toluene
Selectivity	1.17	2.25	1.19	1.06	1.005

Table 2. Confusion matrix for the testing points (in each row, there is the true gas, while in each column, there is the gas identified by the sensing system).

	Acetone	Air	Benzene	Ethanol	Toluene
Acetone	2				
Air		5			
Benzene			3		
Ethanol				3	
Toluene					3

Table 3. Average percentage error calculated for each gas.

Gas	Acetone	Benzene	Ethanol	Toluene
% Error	17.9	63.9	70.6	15.4

Table 4. Average percentage error calculated for each gas, limited to concentrations greater than 1 ppm.

Gas	Acetone	Benzene	Ethanol	Toluene
% Error	13.2	29.4	18.2	14.7